공학석사학위 논문

Performance Improvement of Smart Fin with Piezoelectric Actuator under High Speed Flight Condition

고속 비행 환경에서의 압전 지능형 조종익 성능 개선

2015 년 2 월

서울대학교 대학원

기계항공공학부

노 인 선

Performance Improvement of Smart Fin with Piezoelectric Actuator under High Speed Flight Condition

지도교수 신 상 준

이 논문을 공학석사 학위논문으로 제출함

2014 년 12 월

서울대학교 대학원

기계항공공학부

노 인 선

노인선의 공학석사 학위논문을 인준함

2015 년 2 월

위 원 장 _____

부 위 원 장 _____

위 원 _____

Abstract

Performance Improvement of Smart Fin with Piezoelectric Actuator under High Speed Flight Condition

Inn-Sun Roh

Mechanical and Aerospace Engineering

The Graduate School

Seoul National University

In order to substitute a conventional fin operated by hydraulic actuator, structural analysis of three smart fins embedded with single crystal composite piezoelectric actuators was attempted in this thesis. Structural analysis on piezoelectric actuators employed on the present smart fins using ANSYS showed good correlation with the in-house MATLAB simulation based on classical laminated plate theory, and experimental result. Structural behaviors were analyzed regarding the resulting deflections for each smart fin under specific voltage input. In addition, computational fluid dynamics analysis was conducted on the structures so as to derive the final deflection under aerodynamic load of Mach number 0.5 flight. The present designs and analysis will be extend-ed to future applications such as the control surface component in the wing structures of the unmanned air vehicle and commercial aircraft.

……

keywords : Smart fin, piezoelectric actuator, structural analysis, computational fluid dynamics

***Student Number* : 2013 - 20670**

Table of Contents

List of Figures

List of Tables

Nomenclature

S° = Mid-plane extensional strains

κ = Mid-plane curvature strains

A = Extensional stiffness matrix

B = Coupling stiffness matrix

D = Bending stiffness matrix

N^A = Actuator-induced force

M^A = Actuator-induced moment

e_t = Transpose of piezoelectric induced stress constant Matrix

E = Electric field across the laminate

k = Ply number from the bottom

c^E = Stiffness at constant electric field

s^E = Compliance at constant electric field

$\mathbf{K}$ = Stiffness matrix

$\mathbf{M}$ = Mass matrix

ω = Frequency

Ψ = Modal matrix

ζ = Modal damping ratio

$\mathbf{x}(\omega)$ = Response of a system

$\mathbf{F}(\omega)$ = Excitation force

$\mathbf{H}(\omega)$ = Displacement of a system

$\mathbf{Q}_{hh}$ = Generalized aerodynamic force

q = Modal participants factor

p = Modal force

D = Electric flux

S_m = Source

x = Axial coordinate

r = Radial coordinate

v_x = Axial velocity

v_r = Radial velocity

p = Static pressure

$\rho\vec{g}$ = Gravitational body force

$\vec{F}$ = External Body forces

I. Introduction

1.1 Background of the thesis

Development of composite materials has progressed because of their better physical properties such as longer lifetime, high strength and stiffness to weigh ratio, excellent fatigue properties and corrosion resistance, etc. Such enhancement of the material property was widely accepted in the aerospace engineering field starting from military and spun off to the commercial field. Starting from the first commercial product under the trade name Arall (Aramid Reinforced Aluminum Laminates) was launched by ALCOA in 1982, importance and application of the composite materials for aerospace engineering had been growing ever since to Airbus A380[1]. (Fig. 1.1)

Among the composite materials, smart material has been discovered and experimented in laboratories using fibre optics and piezoelectric sensors and actuators. Main applications that have been pursued are structural health monitoring, vibration and noise control, aerodynamic flow manipulation through surface modification, smart actuation of control surfaces [2].

Piezoelectricity is the ability of certain crystalline materials to develop an electric charge proportional to a mechanical stress, which was discovered by J. and P. Curie in 1880 [3]. Soon, converse effect, a geometric strain proportional to an applied voltage was also discovered, leading to further applications in sensors and actuator fields, and tested both analytically and experimentally.[4]

Structures utilizing this unique property are called intelligent structures, or smart structures. They are a subset of a much larger field of research, as shown in Fig. (1.2). Those structures which have actuators distributed through-out are defined as adaptive or, alternatively, actuated. Classical examples of such mechanically adaptive structures are robotic systems with manipulators and end effectors.

Structures which have sensors distributed throughout are a subset referred to as sensory. These structures have sensors which might detect displacements, strains or other mechanical states or properties, electromagnetic states or properties, temperature or heat flow, or the presence or accumulation of damage. Applications of this technology might include damage detection in long life structures.

The structures of overlapped region which contain both

actuators and sensors (implicitly linked by closed-loop control) are referred to as controlled structures. Any structure with the presence of a closed-loop control system is included in this category. A subset of controlled structures are active structures, distinguished from controlled structures by highly distributed actuators which have structural functionality and are part of the load bearing system [5].

Applications include active control system with piezoelectric actuators in order to minimize the vibrations of large flexible structures which are intended to provide stable bases for precision “pointing” in space[6], adaptive optical system as micro-displacement transducer, which is a part of light wave operating radar loaded on space vehicle for mon-itoring earth’s surface[7](Fig. 1.3), sensor for detecting high-velocity impact location on isotropic and composite aircraft panels[8], and so on.

1.2 Summary of the preceding researches

Analysis on the piezoelectric material and its applications on an air vehicle fin have been conducted by the researchers, such as Sahin [9], Rabinovitch [10], and Mehrabian[11]. As shown in Fig. 1.4 which is the research by Mehrabian, a scaled vertical tail of F/A-18 was developed in which piezoelectric actuators were bonded to the surface for optimization of piezoelectric actuators in vibration supression.

Improvement of the aerodynamic performances while using less actuation and maintaining sleek airfoil shape after deformation for energy efficiency has been a well-noted objective to pursue. In the technical note by Seifert, et al. [12], surface-mounted piezoelectric actuators are used to excite the turbulent boundary layer upstream of separation, where the actuators interact directly with the boundary layer.

Active piezoelectric fins, also called smart fins for flight vehicles with piezoelectric actuators embedded were analyzed and suggested by many researchers. Rabinovitch [13, 14] also introduced analytical modelling and design concepts of the smart fins and a design which rotates around the hinge by

two piezoelectric actuators. (Figs. 1.5, 1.6) Mani and Singh [15] also suggested a smart fin which morphs its cross-sectional shape to create a bent shape which induces aerodynamic forces instead of by rotating around the hinge. (Fig. 1.7)

Researches using computational fluid dynamics (CFD) have been conducted by Gern [16], Chinnasamy [17], and others to prove the aerodynamic advantages of a smooth airfoil shape. Other analytical approach, such as Bent [18], was used to formulate the present analysis to predict its accurate behavior. It is an advanced material well beyond the limitation of the conventional PZT piezoelectric material, which has been developed and utilized over 80 years. Typically, PMN-PT material shows enhanced properties such as electromechanical coupling factor K_{33} and piezoelectric constants d_{31} and d_{33}.

Dynamic aeroelastic instabilities, such as flutter, involve the interaction of aerodynamic, inertia, and elastic forces of flight structures. Because flutter may cause disastrous structural failures in flight, the prediction of stability boundary and the suppression of flutter are very important analysis issues for flight structures. By using piezoelectric actuators,

measurement and suppress the flow-induced vibrations caused by interactions between fluid and structures were examined by Kim, et al. [19] Experimental research was also conducted by Raja [20]. (Fig. 1.8) As the design proposed by Barret[21], structure which has low stiffness has possibility for lower flutter speed, and it would easily lead to instability. Thus it is necessary to conduct flutter analysis for the design candidates for their reliability to be operable under given flight condition.

1.3 Purpose and scope of the thesis

In this thesis, smart fin designs for targeted deflection angle of 10° are proposed and analyzed by simulating their operating conditions. Both structural and aerodynamic analysis was conducted to show their simulated performance and suggest the probable choice for further study. Regarding the present single-crystal piezoelectric material-embedded smart fin, its structural behavior was analyzed and compared with the existing numerical results. Actuation of the present smart fin structures targeted the trailing edge deflection of 10° with respect to the chord position.

In this thesis, a smart fin structure with single crystal

piezoelectric material was analyzed. Single-crystal piezoelectric material used presently was PMN-29PT. By applying classical laminated plate theory, an in-house MATLAB code was developed and used to compare the bending deflection result of the piezoelectric actuator with analytical result by finite element method based analysis software, and experimental result. Bimorph piezoelectric actuator was analyzed using ANSYS structural analysis to check and verify the deflection behavior and performance compared with in-house MATLAB code based on the classical laminated plate theory, and experimental results. After the analysis of bimorph actuator was completed, two smart fin designs embedded with the actuators were first analyzed without any external loads, only showing structural behavior resulted by actuators, and then derived that of the smart fins under Mach number 0.5 flight by deriving the pitching moment induced by aeroynamic forces upon the deflected airfoil shape.

After the validation of the piezoelectric actuator, four smart fins embedded with it were analyzed using commercial software, ANSYS. Simulated analysis using ANSYS includes structural analysis without any external load but piezoelectric actuation force, and aerodynamic analysis under specific flight condition, Mach number 0.5 to find each of their defle-

ction performance under given aerodynamic flight condition.

In Chapter 2, theoretical background regarding classical laminated plate theory which was the basis for the validation of piezoelectric actuator deflection result and theories appli-ed in the commercial analysis software used for this thesis are explained.

Chapter 3 displays aspects of single crystal piezoelectric actuator and four smart fins, of which structural and aerodynamic analysis results by using commercial software ANSYS are presented and compared in Chapter 4.

Chapter 5 concludes the thesis with overall summary of the result and suggests the possible future works.

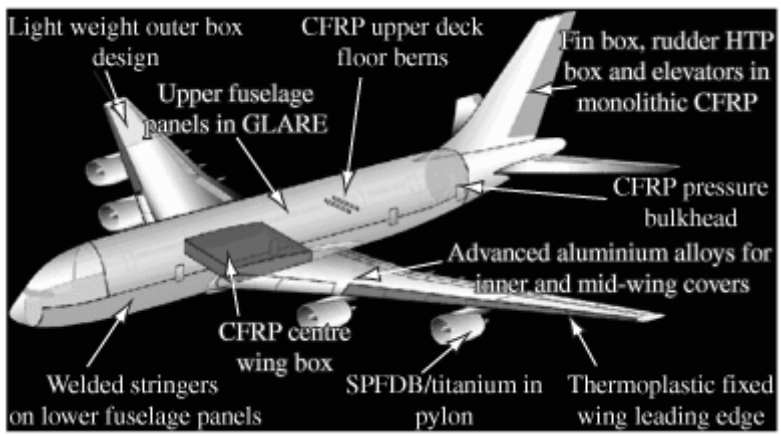

Figure 1.1 Metal/Fiber application in A380 from Airbus[1]

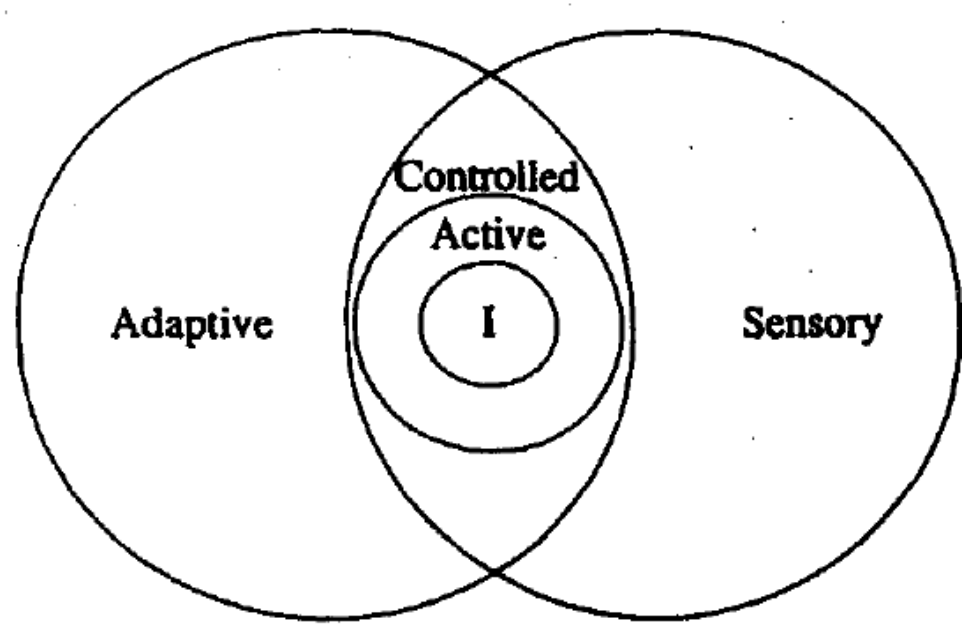

Figure 1.2 Intelligent structures as a subset of active and controlled structures[5]

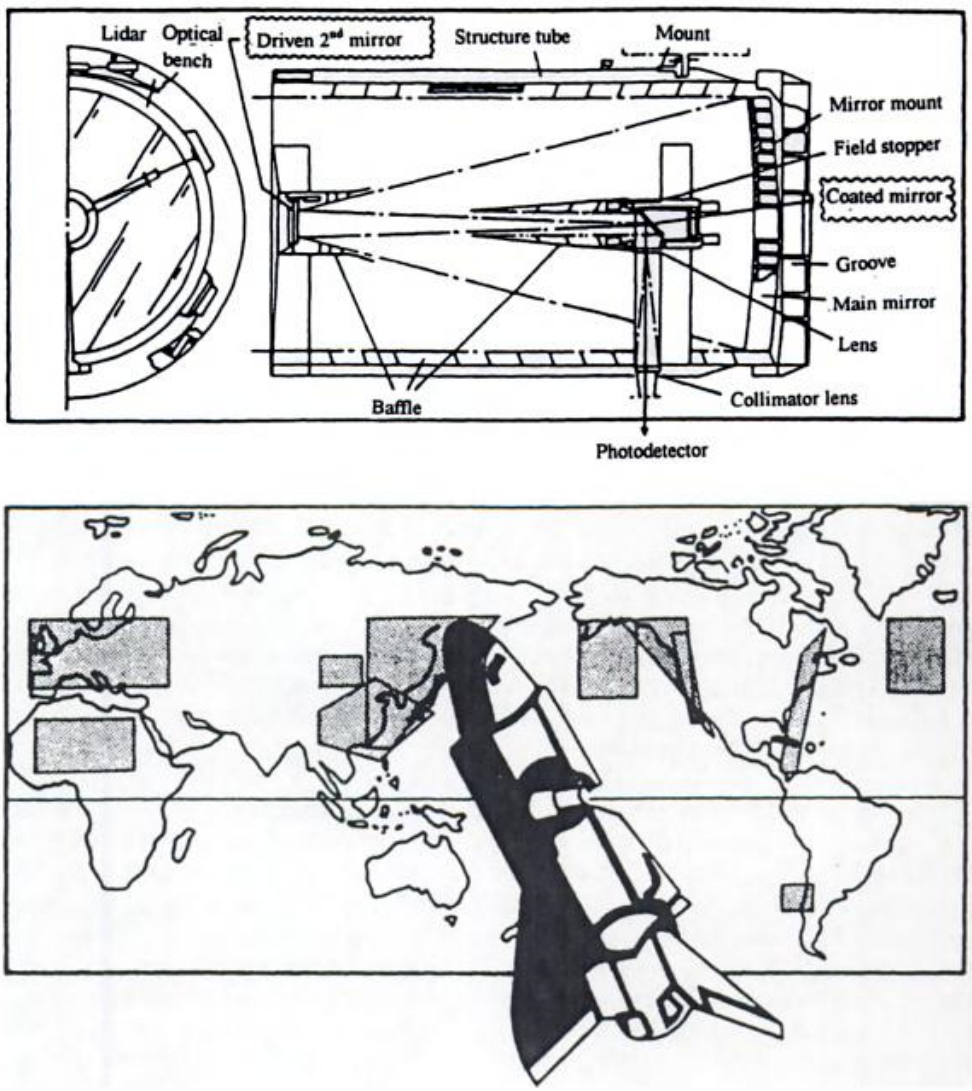

Figure 1.3 Shuttle lidar(prototype) and location of the positioner using piezoelectric actuator[6]

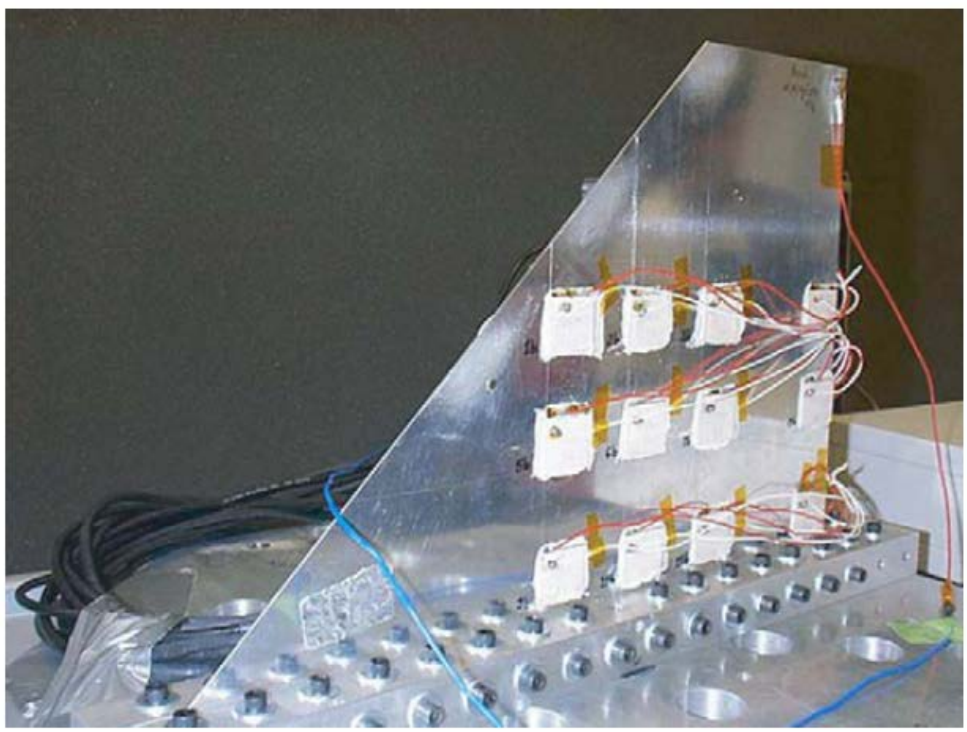

Figure 1.4 Experimental setup of the flexible fin with piezoelectric actuators[11]

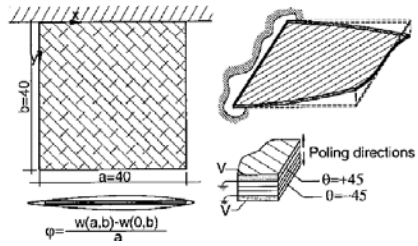

(a) Twist actuation of a cantilevered fin

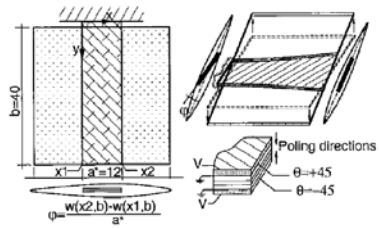

(b) Twist actuation of a central shaft

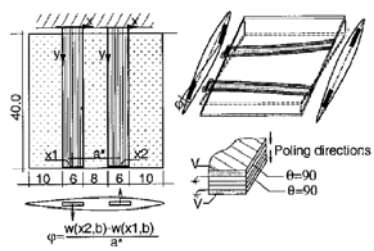

(c) Anti-symmetric bending in parallel configuration;

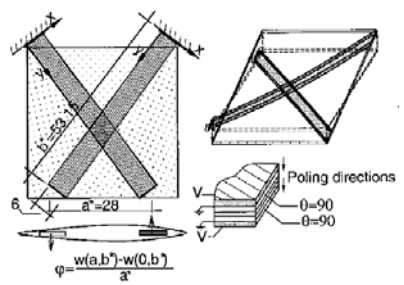

(d) Anti-symmetric bending in diagonal configuration

Figure 1.5 Smart fin designs suggested in Ref. 13

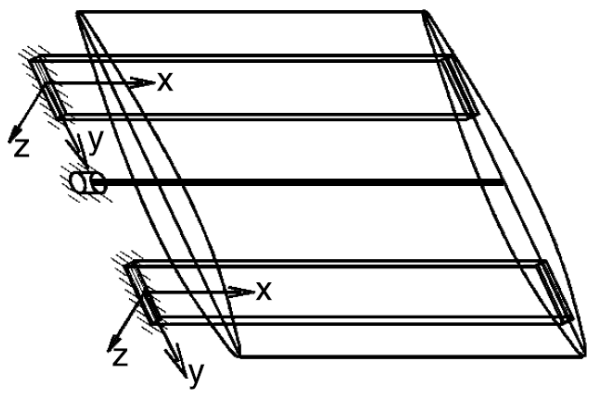

(a) Undeformed shape

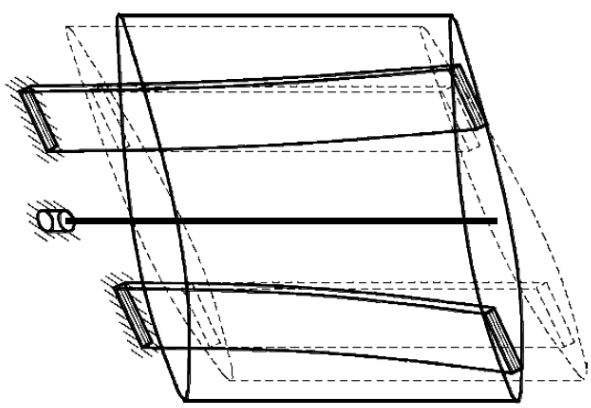

(b) Deformed shape

Figure 1.6 Smart fin designs suggested in Ref. 14

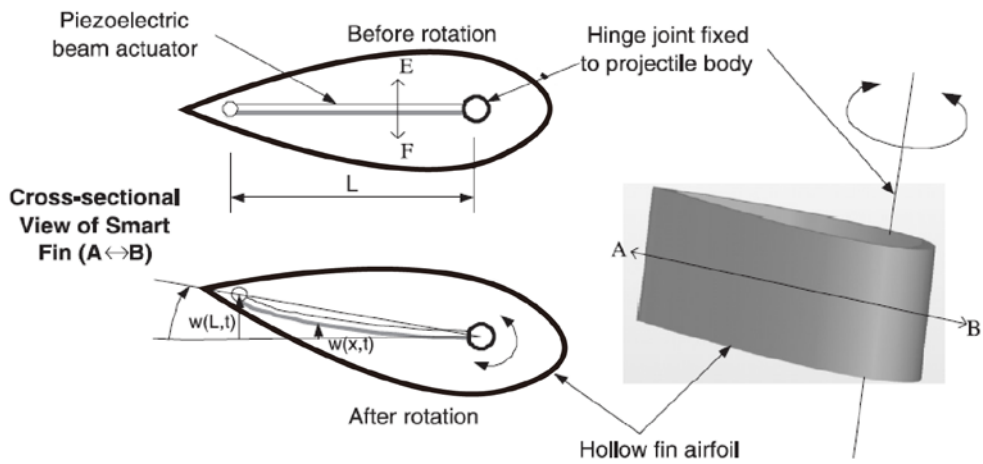

Figure 1.7 Smart fin designs suggested in Ref. 15

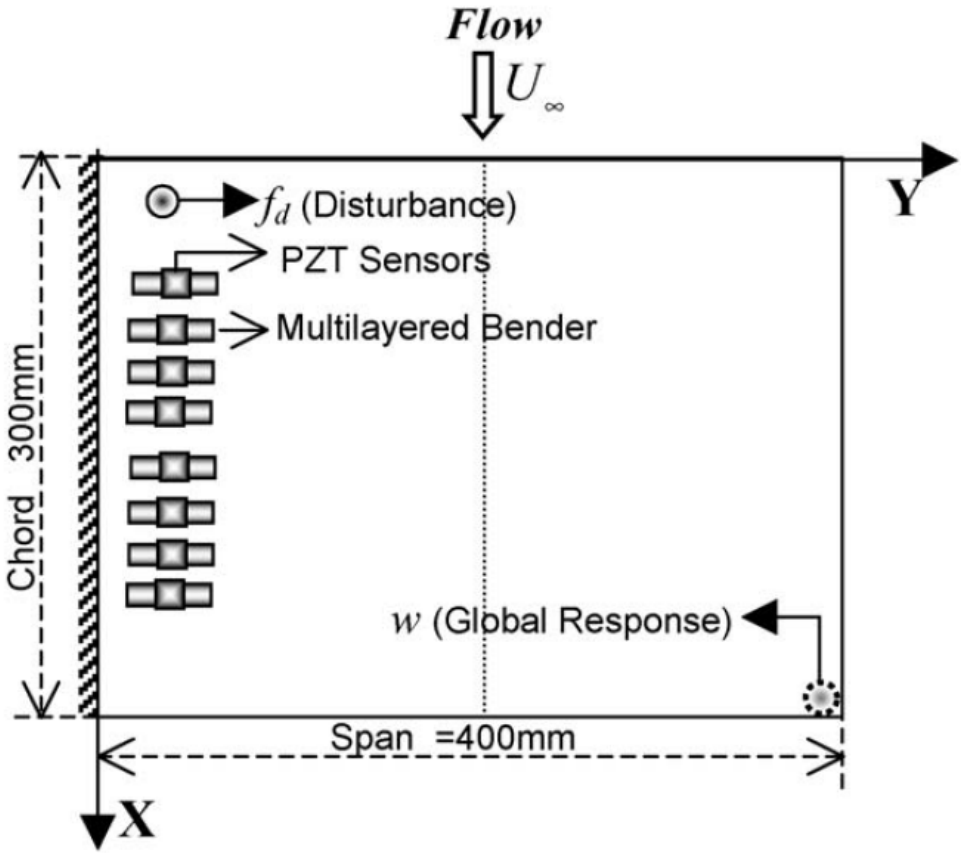

Figure 1.8 Active composite plate [17]

II. Theoretical Backgrounds

In this thesis, a number of analytical tools were used to derive the result. For the piezoelectric actuator, Classical Laminated Plate Theory was applied to build in-house code to verify the result from commercial software using ANSYS, and experimental result. All four Design Candidates were analyzed using ANSYS software for structural analysis and computational fluid dynamic analysis by Fluent to derive aerodynamic load. For Design Candidate 3, natural frequencies for each mode shape were derived using MSC. NASTRAN and applied to ZAERO in order to derive the damping and frequency behavior of each mode, eventually acquiring flutter characteristics.

2.1 Classical Laminated Plate Theory

In order to obtain accurate analytical prediction, an in-house program was developed based on the classical theory of the composite laminated plate and piezoelectric actuation mechanics, suggested by Bent [18]. However, the application of the theory was confined to the piezoelectric actuator only

because of the structural complexity and unrelated material property of the overall structure of the fins. Classical laminated plate theory (CLPT) introduces the stress-strain relationship for the composite material, as shown in Fig. (2.1), with the following stiffness matrix [18],

$$\begin{Bmatrix} \mathrm{S}^{o} \\ \kappa \end{Bmatrix} = \begin{bmatrix} \mathrm{A} & \mathrm{B} \\ \mathrm{B} & \mathrm{D} \end{bmatrix}^{-1} \begin{Bmatrix} \mathrm{N}^{A} \\ \mathrm{M}^{A} \end{Bmatrix} \tag{2.1}$$

where S^{o} is the strain vector for the mid-plane strains, and κ is the curvature strains. N^{A} , M^{A} is the force and moment produced by the piezoelectric layer(s), respectively, as described in Eq. (2.2).

$$\begin{aligned} N^{A} &= \sum_{k=1}^{n_A} (\mathrm{e}_t E_3)_k ((x_3)_k - (x_3)_{k-1}) \\ M^{A} &= \frac{1}{2} \sum_{k=1}^{n_A} (\mathrm{e}_t E_3)_k ((x_3)_k^2 - (x_3)_{k-1}^2) \end{aligned} \tag{2.2}$$

In the stiffness matrix, each component is as follows.

$$
\begin{aligned}
[\mathrm{A}] &= \sum_{k=1}^{n} (\mathrm{c}^{E})_k ((x_3)_k - (x_3)_{k-1}) \\
[\mathrm{B}] &= \frac{1}{2} \sum_{k=1}^{n} (\mathrm{c}^{E})_k ((x_3)_k^2 - (x_3)_{k-1}^2) \\
[\mathrm{D}] &= \frac{1}{3} \sum_{k=1}^{n} (\mathrm{c}^{E})_k ((x_3)_k^2 - (x_3)_{k-1}^3)
\end{aligned}
\tag{2.3}
$$

with

$$
\mathrm{c}^{E} = (\mathrm{s}^{E})^{-1} \tag{2.4}
$$

$$
\mathrm{s}^{E} = \begin{bmatrix}
s_{11}^{E} & s_{12}^{E} & s_{13}^{E} & 0 & 0 & 0 \\
s_{12}^{E} & s_{22}^{E} & s_{23}^{E} & 0 & 0 & 0 \\
s_{13}^{E} & s_{23}^{E} & s_{33}^{E} & 0 & 0 & 0 \\
0 & 0 & 0 & s_{44}^{E} & 0 & 0 \\
0 & 0 & 0 & 0 & s_{55}^{E} & 0 \\
0 & 0 & 0 & 0 & 0 & s_{66}^{E}
\end{bmatrix} \tag{2.5}
$$

n is the number of total plies in the laminate, n_A is the number of the piezoelectric layers, e_t is the transpose of the piezoelectric induced stress constant matrix, and E_3 is the

electric field across the laminates in x_3 direction.

Based on the Classical Laminated Plate Theory, in-house MATLAB code was built for the verification of results by other analysis methods.

2.2 Open and closed circuit condition of piezoelectric components

For the case of open circuit condition of a piezoelectric component, the charges of the electrodes are not free to move and are disposed so that they face those present on the dielectric. Therefore, no electric flux D is present. (Fig. 2.2) For the closed circuit condition, no electric field is present because both electrodes have the same electric potential. The charges move in the metallic part in such a way that only negative charges are present on the top electrode and positive ones on the lower electrode. The experimental evidence demonstrates that for the open circuit case the stiffness of the material is greater than that in the closed circuit case. The reason for this difference is that in closed circuit, the charges on the electrodes cancel those on the piezoelectric surfaces, the stress does not have to work against the electrical forces,

since no polarization is present if electrodes are included. On the other hand, in the open circuit case stress has also to overcome the forces between electric charges, because polarization is also still effective if the electrode planting is included. This explains the physical evidence that the stiffness at zero D is greater than that at zero E. (Eqs. (2.6) and (2.7)) [23]

$$s^D = s^E - d_t(\varepsilon^T)^{-1}d \tag{2.6}$$

$$c = (s)^{-1} \tag{2.7}$$

The change of stiffness of the piezoelectric structure under two different conditions was derived and applied for flutter analysis in order to compare the flutter characteristics result of Design Candidate 3.

2.3 Analysis theories used in ANSYS

ANSYS static structural analysis was used for analyzing the actuation of piezoelectric material and overall deformation of structure. For a linear static structural analysis, the displacements {x} are solved for in the matrix equation under the assumption that stiffness matrix [K] is constant so that linear elastic material behavior is assumed, small deflection theory is used, and some nonlinear boundary conditions may be included. (Eq. (2.8)) {F} is statically applied so that there are no time-varying forces to be considered, and no inertial effects (mass, damping) are included [24].

$$[K]\{x\}=\{F\} \tag{2.8}$$

Contact analysis was applied to simulate the blockings of components in the structures. Frictionless conditions were applied by using Augmented Lagrange method. Summary of the contact types offered in ANSYS is shown in Table 2.1 [24].

2.4 Analysis theories used in ANSYS Fluent

In this thesis, inviscid flow condition was assumed using ANSYS Fluent. Inviscid flow analyses neglect the effect of viscosity on the flow and are appropriate for high-Reynolds-number applications where inertial forces tend to dominate viscous forces. This assumption is appropriate for an aerodynamic analysis of some high-speed projectiles[25].

For inviscid flows, ANSYS Fluent solves the Euler equations. The mass conservation equation is the same as for a laminar flow, but the momentum and energy conservation equations are reduced due to the absence of molecular diffusion.

The equation for conservation of mass, or continuity equation, can be written as follows:

$$\frac{\partial \rho}{\partial t} + \nabla \cdot (\rho \vec{v}) = S_m \tag{2.9}$$

Eq. (2.9) is the general form of the mass conservation equation and is valid for incompressible as well as compressible flows. The source S_m is the mass added to the continuous phase from the dispersed second phase (for

example, due to vaporization of liquid droplets) and any user-defined sources.

For two-dimensional axisymmetric geometries, the continuity equation is given by

$$\frac{\partial \rho}{\partial t} + \frac{\partial}{\partial x}(\rho v_x) + \frac{\partial}{\partial r}(\rho v_r) + \frac{\rho v_r}{r} = S_m \qquad (2.10)$$

where x is the axial coordinate, r is the radial coordinate, v_x is the axial velocity, and v_r is the radial velocity.

Conservation of momentum is described by

$$\frac{\partial}{\partial t}(\rho \vec{v}) + \nabla \cdot (\rho \vec{v} \vec{v}) = -\nabla p + \rho \vec{g} + \vec{F} \qquad (2.11)$$

where p is the static pressure and $\rho \vec{g}$ and $\vec{F}$ are the gravitational body force and external body forces (for example, forces that arise from interaction with the dispersed phase), respectively. $\vec{F}$ also contains other model-dependent source terms such as porous media and user-defined sources.

For 2D axisymmetric geometries, the axial and radial

momentum conservation equations are given by

$$\frac{\partial}{\partial t}(\rho v_x) + \frac{1}{r}\frac{\partial}{\partial x}(r\rho v_x v_x) + \frac{1}{r}\frac{\partial}{\partial r}(r\rho v_r v_x) = -\frac{\partial p}{\partial x} + F_x \quad (2.12)$$

and

$$\frac{\partial}{\partial t}(\rho v_r) + \frac{1}{r}\frac{\partial}{\partial x}(r\rho v_x v_r) + \frac{1}{r}\frac{\partial}{\partial r}(r\rho v_r v_r) = -\frac{\partial p}{\partial r} + F_r \quad (2.13)$$

where

$$\nabla \cdot \vec{v} = \frac{\partial v_x}{\partial x} + \frac{\partial v_r}{\partial r} + \frac{v_r}{r} \quad (2.14)$$

Conversion of energy is described by

$$\frac{\partial}{\partial t}(\rho E) + \nabla \cdot (\vec{v}(\rho E + p)) = -\nabla \cdot (\sum_j h_j J_j) + S_h \quad (2.15)$$

2.5 Analysis theories used in MSC. NASTRAN

NASTRAN assembles the system's mass and stiffness matrices, leading to a set of differential equations, displayed by Eq. (2.16), already transformed in the frequency domain (damping is neglected at first).

$$\mathbf{M}\,\ddot{\mathbf{x}} + \mathbf{K}\,\mathbf{x} = \mathbf{f}(\omega) \tag{2.16}$$

Secondly, NASTRAN solves the characteristic Eq. (2.17) for eigenvalues and computes the corresponding eigenmodes.

$$\det\left(\mathbf{K} - \omega^2\mathbf{M}\right) = 0 \tag{2.17}$$

With the separation approach in Eq. (2.18), a modal transformation [26, 27] is performed, which diagonalizes the system from Eq. (2.16), using the orthogonality properties of the eigenvectors in the modal matrix Ψ, consisting of the calculated eigenvectors.

$$\mathbf{x} = \Psi\,\mathbf{q}(\omega)$$

with

$$\Psi = [\psi_1, \psi_2, \psi_3, \ldots, \psi_N] \tag{2.18}$$

Hereby the system, consisting of N degrees of freedom, is decoupled, leading to a system of N single-mass oscillators, with each oscillator representing an eigenmode of the system in general coordinates q_i in Eq. (2.19)

$$m_i \ddot{q}_i(\omega) + k_i q_i(\omega) = p_i(\omega) \tag{2.19}$$

Here, m_i is the modal mass, k_i the modal stiffness, and $p_i = \psi_i^{\mathrm{T}} \cdot \mathbf{f}$ the modal force. With the eigen-frequencies $\omega_i^2 = k_i / m_i$, Eq. (2.19) can be transformed to Eq. (2.20). Furthermore, damping can be introduced by a modal damping ratio ζ_i (Eq. (2.21), [28]).

$$\ddot{q}_i(\omega) + \omega_i^2 q_i(\omega) = \frac{p_i(\omega)}{m_i} \tag{2.20}$$

$$q_i(\omega) + 2\zeta_i \dot{q}_i(\omega) + \omega_i^2 q_i(\omega) = \frac{p_i(\omega)}{m_i} \tag{2.21}$$

The solution of this differential equation is well known and given by Eq. (2.22).

$$q_i(\omega) = \frac{1}{\omega_i^2 - \Omega_i^2 + i2\zeta\omega_i\Omega_i} \cdot \frac{\hat{p}_i(\omega)}{m_i} \qquad (2.22)$$

Then, the solution for the system is a linear combination of the solutions for all oscillators (Eq. (2.23)).

$$\mathbf{x}(\omega) = \sum_{i=1}^{N} \psi_i q_i(\omega) \qquad (2.23)$$

The frequency response function is defined as the ratio of the response of a system $\mathbf{x}(\omega)$ (displacement, velocity, acceleration) to its excitation force $\mathbf{F}(\omega)$. The Frequency Response Function (FRF) for displacement of the system is given by Eq. (2.24).

$$\mathbf{H}(\omega) = \frac{\mathbf{x}(\omega)}{\mathbf{F}(\omega)} = \sum_{i=1}^{N} \psi_i \cdot \frac{1}{\omega_i^2 - \Omega_i^2 + i2\zeta_i\omega_i} \cdot \frac{\psi_i^T}{m_i} \qquad (2.24)$$

Thus, the FRF for the k-th node (degree of freedom) with

a single excitation force at j-th DOF can be calculated by Eq. (2.25) [29].

$$H_k(\omega) = \sum_{i=1}^{N} \frac{\psi_{ik} \cdot \psi_{ij}}{m_i(\omega_i^2 - \Omega_i^2 + i2\zeta_i\omega_i)} \tag{2.25}$$

2.6 Analysis theories used in ZAERO

With the modal analysis result acquired from NASTRAN, ZAERO was used to analyze the flutter characteristics of the given structure.

The ZAERO flutter module contains two flutter solution techniques: the k-method and the g-method. The g-method is flutter solution method that generalizes the K-method and the p-k method for true damping prediction. It is shown that the p-k method is only valid at the conditions of zero damping, zero frequency, or linearly varying generalized aerodynamic forces ($\mathbf{Q}_{hh}$) with respect to reduced frequency. In fact, if $\mathbf{Q}_{hh}$ is highly nonlinear, it is shown that the P-K method may produce unrealistic roots due to its inconsistent formulation.

The flutter module has a built-in atmospheric table as an option to perform matched-point flutter analysis. Sensitivity

analysis with respect to the structural parameters is also included in the g-method. [30]

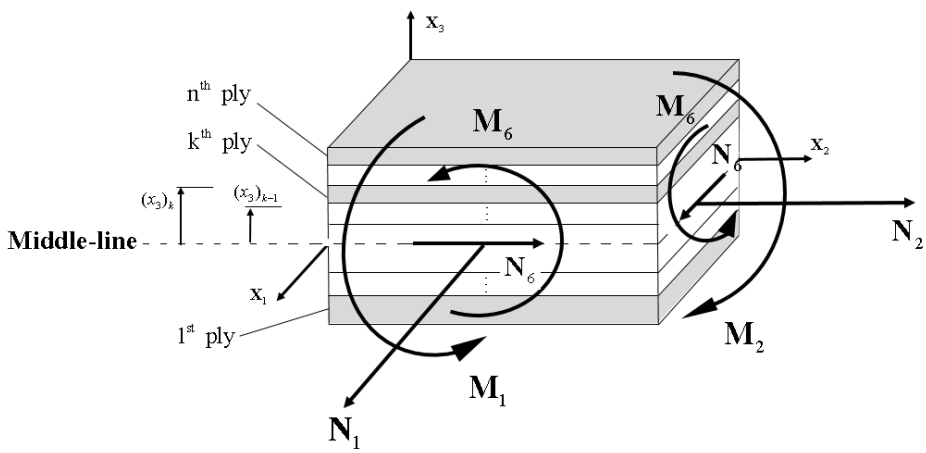

Figure 2.1. Classical laminated plate theory

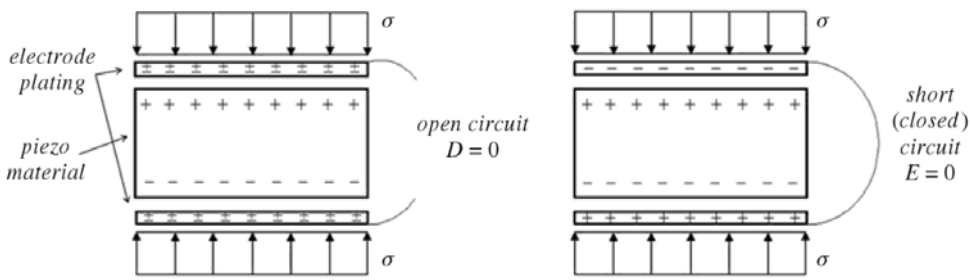

Figure 2.2 Open and closed circuit condition of piezoelectric under compression

Table 2.1 Summary of contact types and options available in ANSYS Simulation [24]

Contact Geometry	Solid Body Face (Scope = Contact)	Solid Body Edge (Scope = Contact)	Surface Body Face (Scope = Contact)	Surface Body Edge (Scope = Contact)
Solid Body Face	All types	Bonded, No Separation	Bonded, No Separation	Bonded only
	All formulations	All formulations	All formulations	MPC formulation
(Scope = Target)	Symmetry respected	Asymmetric only	Symmetry respected	Asymmetric only
Solid Body Edge	Not supported for solving[1]	Bonded, No Separation	Not supported for solving[1]	Bonded only
		All formulations		MPC formulation
(Scope = Target)		Asymmetric only		Asymmetric only
Surface Body Face	Bonded, No Separation	Bonded, No Separation	Bonded, No Separation	Bonded only
(Scope = Target)	All formulations	All formulations	All formulations	Augmented Lagrange, Pure Penalty, and MPC formulation
	Symmetry respected	Asymmetric only	Symmetry respected	Asymmetric only
Surface Body Edge	Not supported for solving[1]	Bonded only	Not supported for solving[1]	Bonded only
(Scope = Target)		MPC formulation		Augmented Lagrange, Pure Penalty, and MPC formulation
		Asymmetric only		Asymmetric only

1 – For Face/Edge contact, faces must always be designated as targets and edges must always be designated as contacts

III. Description of the present smart fin structures

The present smart fin structures were designed using NACA0012 airfoil shape with a chord length of 90 mm, camber length of 10.8 mm, and span length of 14.5 mm for the first design, and 60 mm for the others. Piezoelectric material used in the present structure was PMN-29PT and were laminated to perform bending actuation. Regarding the unimorph actuator, PMN-29PT layer was laminated asymmetrically with respect to the mid-plane, which created the bending moment. Bimorph actuator had symmetric composition of laminate, but bending was induced by applying an opposite voltage input on each layer. Experiment was conducted using two different electrode patterns, closed back bone electrode and open back bone electrode, for the performance comparison. (Figure 3.1)

3.1 Design Candidate 1

Purpose of this design was to utilize the bending deflection of actuators directly. Its simple structural mechanism and stable structure was the primary design points.

It includes one bimorph actuator in the middle and two

unimorph actuators placed symmetrically above and below the middle surface. Total mass of the used PMN-29PT material was 5.18 g. The bimorph actuator connects both the leading and trailing edge. The unimorph actuators and airfoil skins are attached on the leading edge, whereas its left end is not attached on the trailing edge so that it may let these components slide with each other. Therefore, when it is operated, either the upper or lower unimorph actuator, as well as bimorph actuators will slide with respect to the trailing edge. And the upper and lower airfoil skin will slide with respect to each other. Fig. 3.2 illustrates the components used in the present smart fin. Fig. 3.3 shows various views of the fin. And Fig. 3.4 illustrates the actuator lay-up. Table 3.1 summarizes its details.

3.2 Design Candidate 2

This design had been referred to the previous smart fin research by Barret[21]. Main reason for this reference was simple structural aspects with hinge on aerodynamic center, one bimorph piezoelectric actuator as deflection source, and rotation of the entire fin structure without any morphing of cross-sectional airfoil contour. It includes one bimorph

actuator slantly embedded inside the airfoil along the chord line. Total mass of the used PMN-29PT material was 4. 56 g. The hinge is placed on the 1/4 of the chord line in order to take advantage of the simplicity in aerodynamic characteristics. Both hinge and a side of the bimorph actuator will be attached to the flying body. Therefore, when actuator is operated, bimorph actuators will bend up or down, causing the airfoil to create the angle of attack by rotating on its pivot on 1/4 of the chord. Figure 3.5 illustrates the components used in the present smart fin, Fig. 3.6 shows various views of the fin and Fig. 3.7 illustrates the actuator lay-up. Table 3.2 summarizes its details.

3.3 Design Candidate 3

This design was slightly altered from Barret[21] in order to bring the forcing point of the piezoelectric actuator closer to the aerodynamic center in order to take advantage of the characteristic of non-increasing aerodynamic pitching moment of the airfoil with respect to the angle of attack.

Instead of the slanted bimorph actuator, straightened one aligned in span-wise direction was embedded along the chord line inside the hollow space inside the fin. The hinge is pla-

ced on the 1/4 of the chord line in order to take advantage of the characteristic of non-increasing aerodynamic pitching moment of the airfoil with respect to the angle of attack. Both hinge and a side of the bimorph actuator are attached to the vehicle fuselage. Therefore, when actuator is operated, bimorph actuator will bend up or down, causing the airfoil to create the angle of attack by rotating on its pivot on 1/4 of the chord. Total mass of the used PMN-29PT material was 3.44 g. Figure 3.8 illustrates the components used in the present smart fin, Fig. 3.9 shows various views of the present fin and Fig. 3.10 illustrates the actuator lay-up and Table 3.3 summarizes its details.

3.4 Design Candidate 4

This design was proposed with novel mechanism by arranging the bimorph actuators in crossing manner. Its goal was to amplify the small deflections of actuators by inducing rotation, thus creating higher overall deflection. It includes three bimorph actuators in each gap between the leading edge and connecting component, connecting component and trailing edge. Total mass of the used PMN-29PT material was 2.37 g. Unlike Design Candidate 1, actuators were placed in a crossing

manner in order to maximize the conversion of small bending deflection of the bimorph actuator. Similar mechanism was repeated to amplify the deflection angle of the whole structure. When it is operated, all the bimorph actuators operate to bend upward or downward, causing the connecting component and trailing edge to move upward or downward at the same time. Each component was also restrained its motion by slide-contact region. Figure 3.11 illustrates the components used in the present smart fin, and Fig. 3.12 shows various views of the fin. Two different sizes of rectangular shaped bimorph actuators were designed to fit in the gap between leading edge and connecting component, connecting component and trailing edge. (Figure 3.13) Table 3.4 summarizes its details.

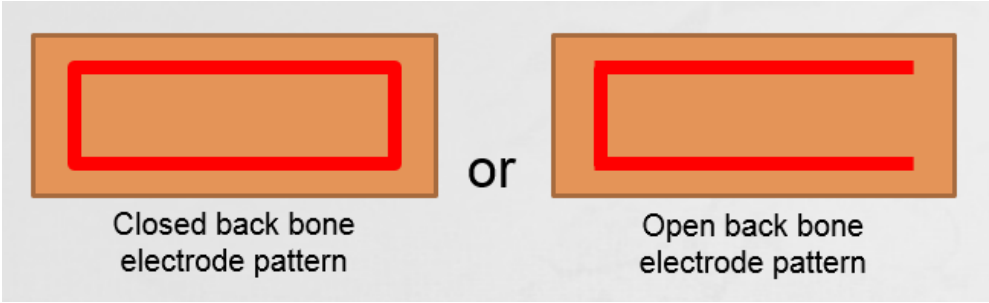

Figure 3.1 Closed and open back bone electrodes

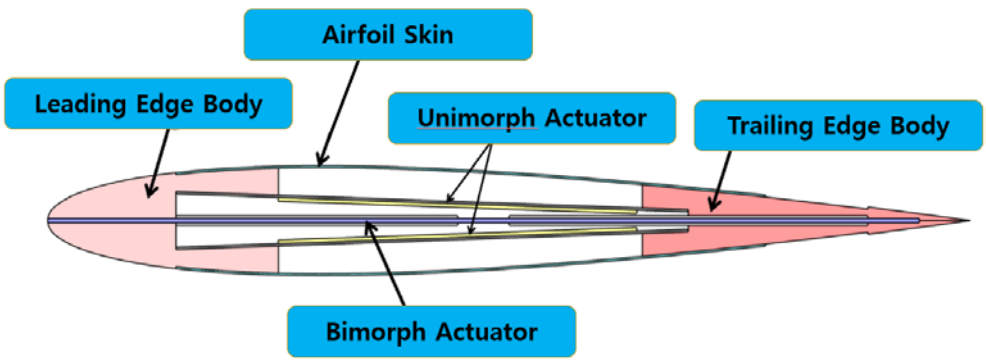

Figure 3.2 Cross-sectional view of the Design Candidate 1

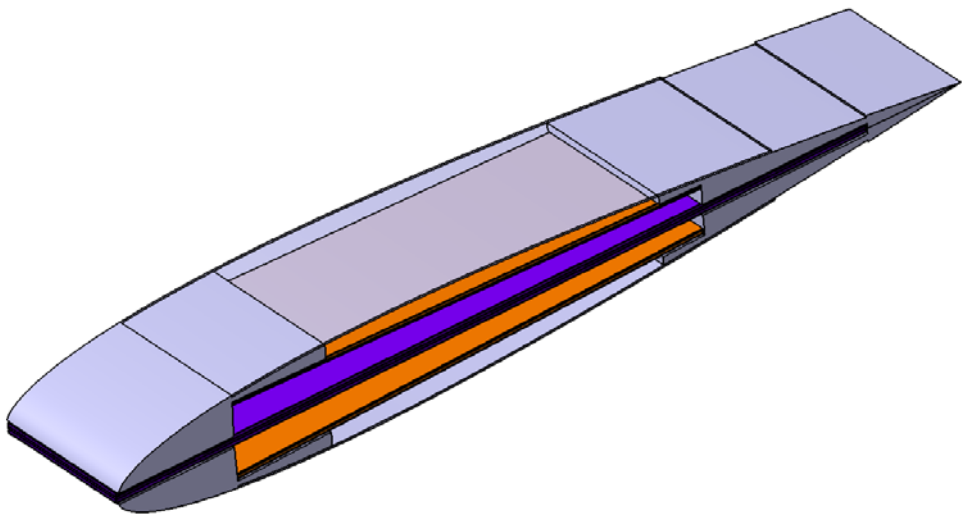

(a) Upper view attached to the vehicle fuselage

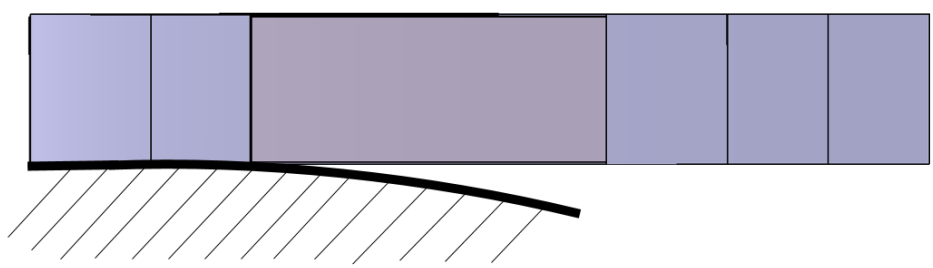

(b) Isometric view

Figure 3.3 Different views of Design Candidate 1

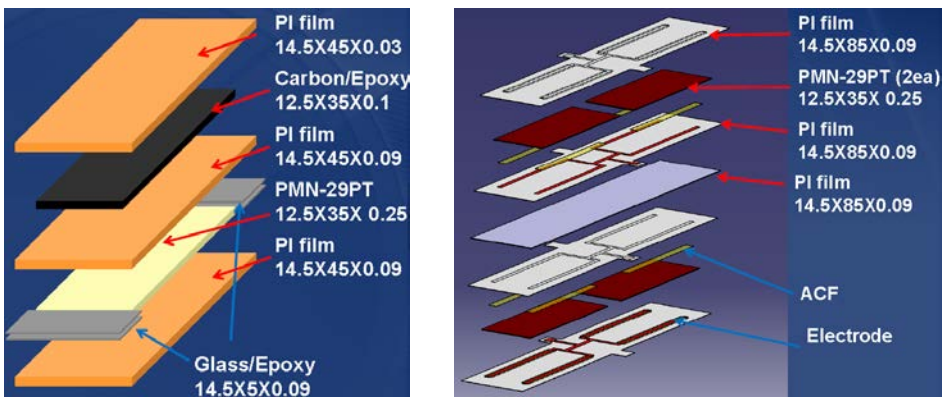

(a) Unimorph actuator (b) Bimorph actuator

Figure 3.4 Lay-up and dimensions of the bimorph actuator in Design Candidate 1

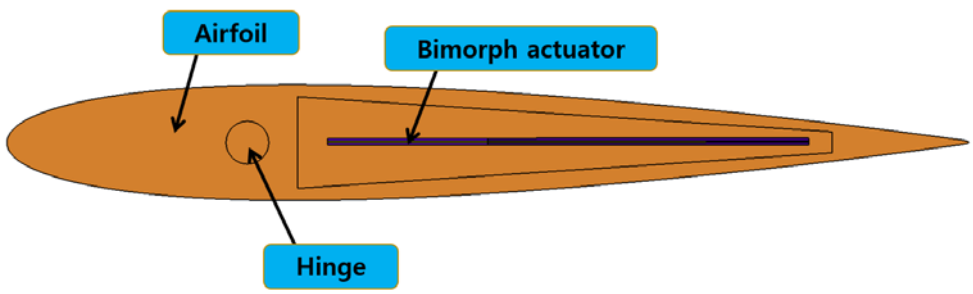

Figure 3.5 Cross-sectional view of the Design Candidate 2

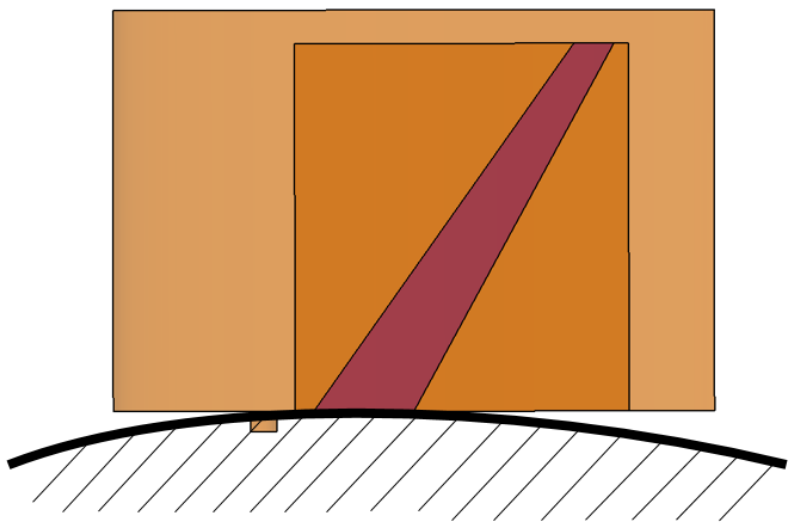

(a) Upper view attached to the vehicle fuselage

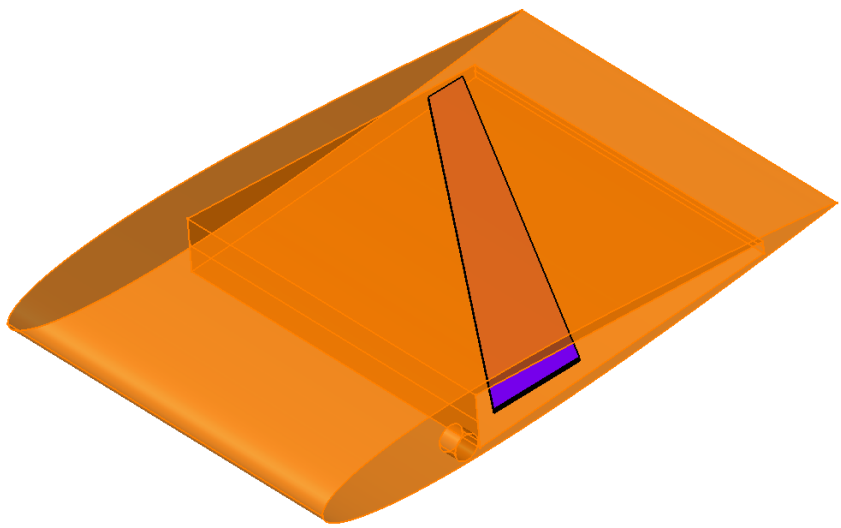

(b) Isometric view

Figure 3.6 Different views of the Design Candidate 2

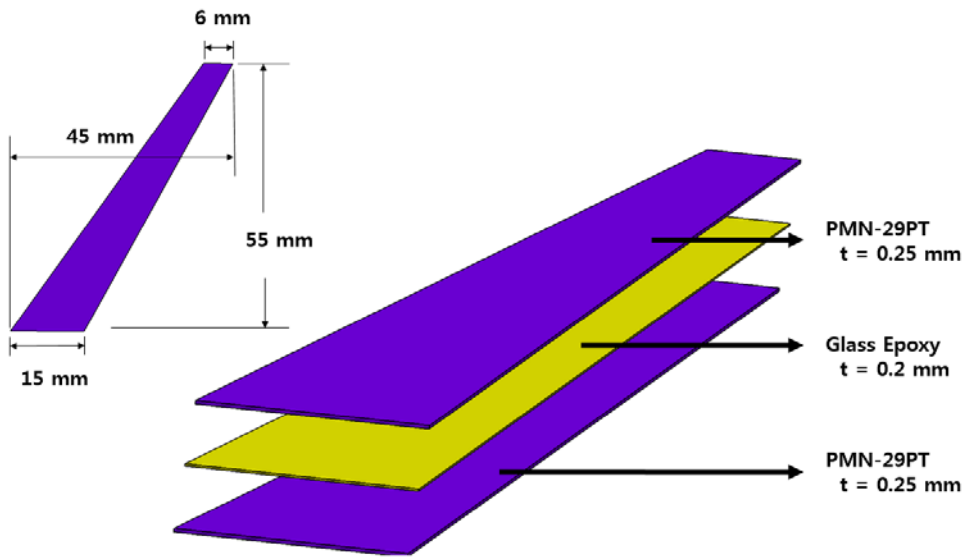

Figure 3.7 Lay-up and dimensions of the bimorph actuator in Design Candidate 2

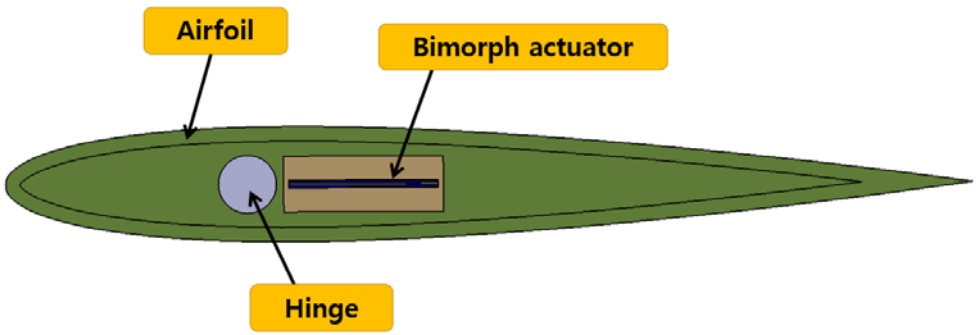

Figure 3.8 Cross-sectional view of the Design Candidate 3

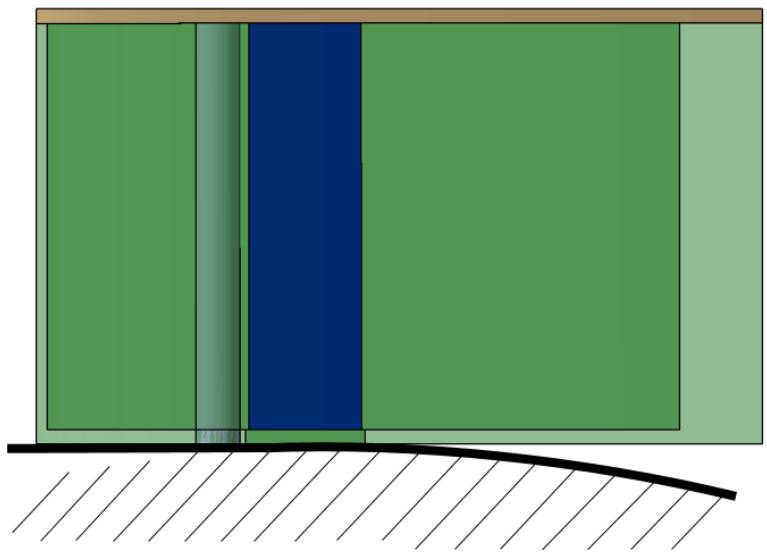

(a) Upper view attached to the vehicle fuselage

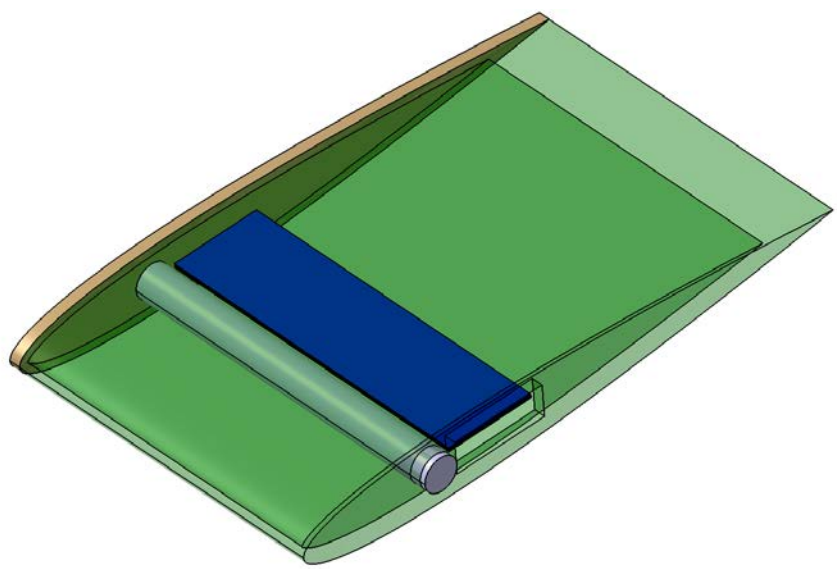

(b) Isometric view

Figure 3.9 Different views of the Design Candidate 3

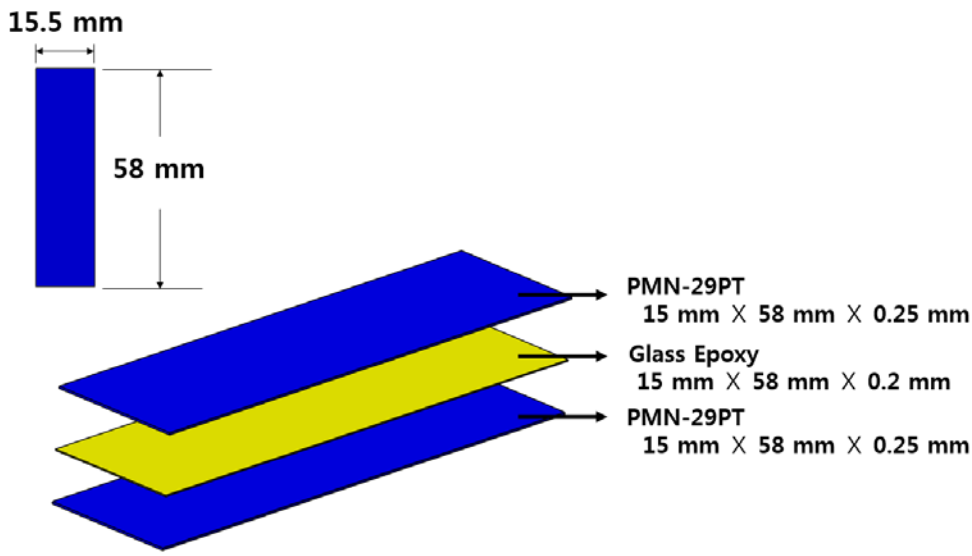

Figure 3.10 Lay-up and dimensions of the bimorph actuator in Design Candidate 3

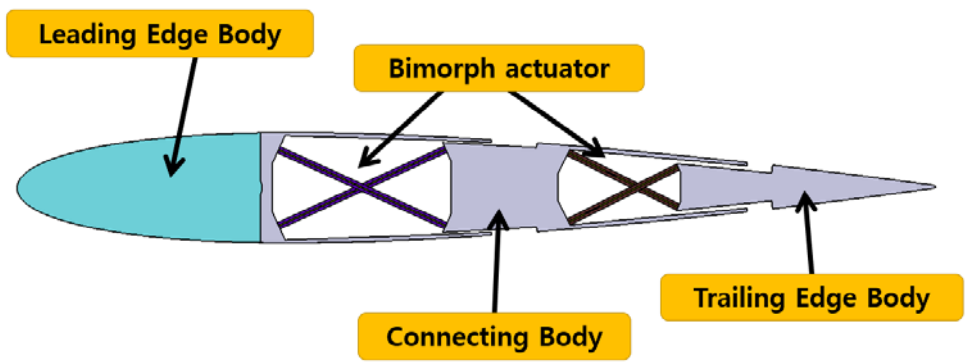

Figure 3.11 Cross-sectional view of the Design Candidate 4

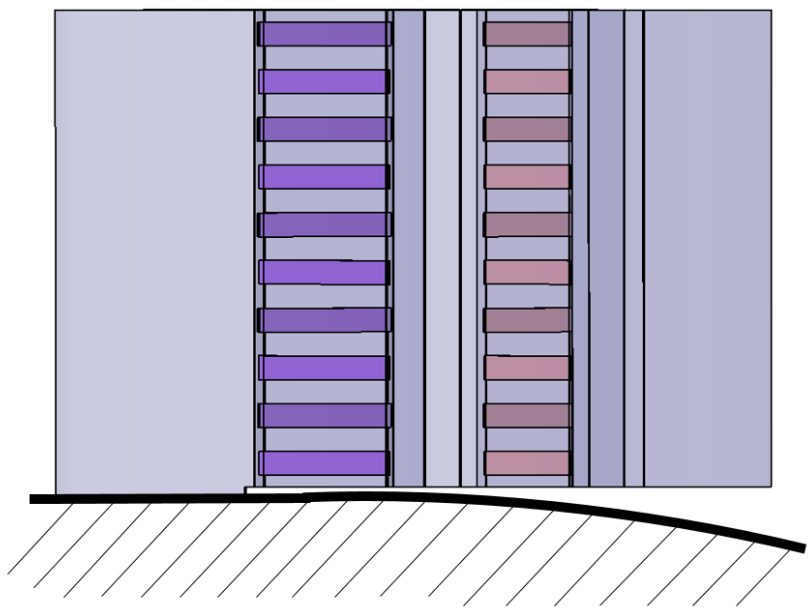

(a) Upper view attached to the vehicle fuselage

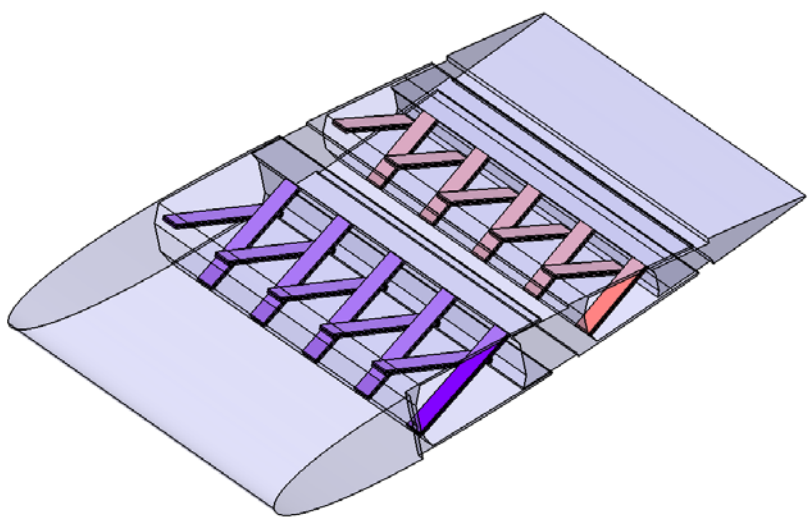

(b) Isometric view

Figure 3.12 Different views of Design Candidate 4

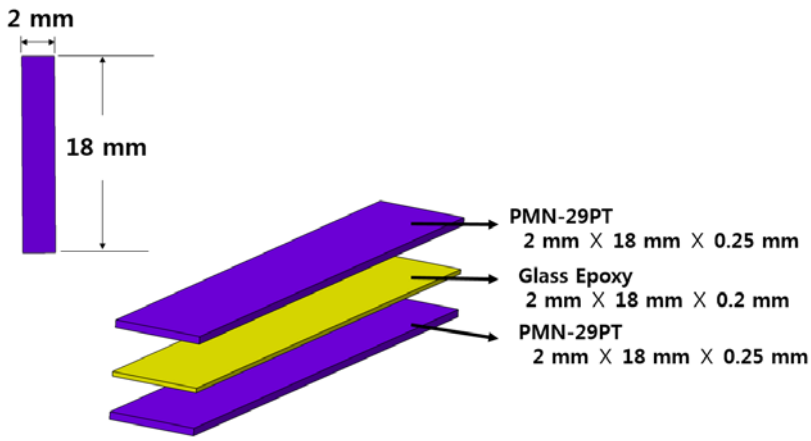

(a) Bimorph actuator used on the front of Design Candidate 4

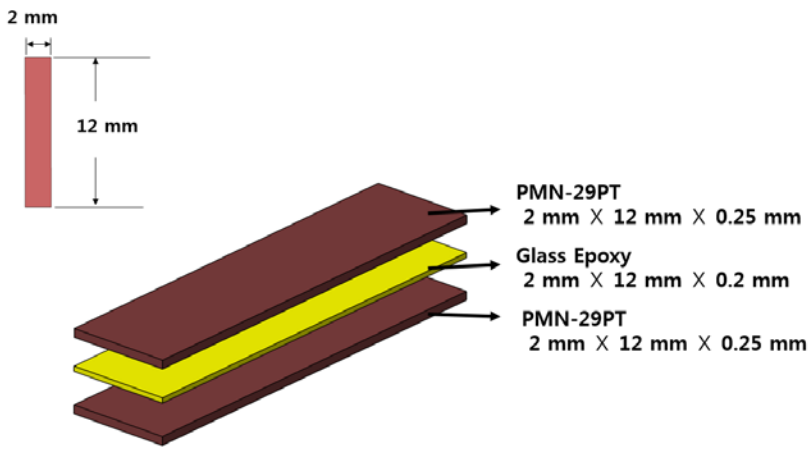

(b) Bimorph actuator used on the back of Design Candidate 4

Figure 3.13 Lay-up and dimensions of the actuators

Table 3.1 Material properties used in the Design Candidate 1 smart fin components [31] [32]

	Parts	Material / Lay-up	Material Property
1	Leading Edge	Aluminum	E_1 = 72 GPa, ν = 0.3
2	Airfoil Skin	Glass/Epoxy	E_1 = 21.7 GPa, ν = 0.3
3	Bimorph Actuator	PI film	E_1 = 3 GPa, ν = 0.3
		PMN-29PT	E_1 = 18.5 GPa, ν = 0.3
		PI film	E_1 = 3 GPa, ν = 0.3
		Glass / Epoxy	E_1 = 21.7 GPa, ν = 0.3
		PI film	E_1 = 3 GPa, ν = 0.3
		PMN-29PT	E_1 = 18.5 GPa, ν = 0.3
		PI film	E_1 = 3 GPa, ν = 0.3
4	Unimorph Actuator	PI film	E_1 = 3 GPa, ν = 0.3
		PMN-29PT	E_1 = 18.5 GPa, ν = 0.3
		PI film	E_1 = 3 GPa, ν = 0.3
		Carbon/Epoxy	E_1 = 212.7 GPa, ν = 0.3
		PI film	E_1= 3 GPa, ν = 0.3
5	Trailing Edge	Aluminum	E_1 = 72 GPa, ν = 0.3

Table 3.2 Material properties used in the Design Candidate 2 components [31, 32]

	Parts	Material / Lay-up	Material Property
1	Airfoil	Glass/Epoxy	E_1 = 21.7 GPa, ν = 0.3
2	Hinge	Glass/Epoxy	E_1 = 21.7 GPa, ν = 0.3
3	Bimorph Actuator	PI film	E_1 = 3 GPa, ν = 0.3
		PMN-29PT	E_1 = 18.5 GPa, ν = 0.3
		PI film	E_1 = 3 GPa, ν = 0.3
		Glass / Epoxy	E_1 = 21.7 GPa, ν = 0.3
		PI film	E_1 = 3 GPa, ν = 0.3
		PMN-29PT	E_1 = 18.5 GPa, ν = 0.3
		PI film	E_1 = 3 GPa, ν = 0.3

Table 3.3 Material properties used in the Design Candidate 3 components [31][32]

	Parts	Material / Lay-up	Material Property
1	Airfoil	Glass/Epoxy	E_1 = 21.7 GPa, ν = 0.3
2	Hinge	Glass/Epoxy	E_1 = 21.7 GPa, ν = 0.3
3	Bimorph Actuator	PI film	E_1 = 3 GPa, ν = 0.3
		PMN-29PT	E_1 = 18.5 GPa, ν = 0.3
		PI film	E_1 = 3 GPa, ν = 0.3
		Glass / Epoxy	E_1 = 21.7 GPa, ν = 0.3
		PI film	E_1 = 3 GPa, ν = 0.3
		PMN-29PT	E_1 = 18.5 GPa, ν = 0.3
		PI film	E_1 = 3 GPa, ν = 0.3

Table 3.4 Material properties used in the Design Candidate 4 components [31] [32]

	Parts	Material / Lay-up	Material Property
1	Leading Edge	Aluminum	E_1 = 72 GPa, ν = 0.3
2	Bimorph Actuator	PI film	E_1 = 3 GPa, ν = 0.3
		PMN-29PT	E_1 = 18.5 GPa, ν = 0.3
		PI film	E_1 = 3 GPa, ν = 0.3
		Glass / Epoxy	E_1 = 21.7 GPa, ν = 0.3
		PI film	E_1 = 3 GPa, ν = 0.3
		PMN-29PT	E_1 = 18.5 GPa, ν = 0.3
		PI film	E_1 = 3 GPa, ν = 0.3
3	Connecting Body	Aluminum	E_1 = 72 GPa, ν = 0.3
4	Trailing Edge	Aluminum	E_1 = 72 GPa, ν = 0.3

IV. Numerical and Experimental Results

Structural analysis of piezoelectric actuator was conducted to verify its bending deflection performance using in-house MATLAB simulations and experimental result. Structural and aerodynamic analysis results for the four smart fin design using ANSYS software are obtained and presented. The result includes analytical, experimental, and simulated bending deflection results of piezoelectric actuator. Deflection angles of the present four smart fins were derived from analysis for comparison.

4. 1. Piezoelectric Actuator

In order to verify the performance of the present piezoelectric actuator, experimental actuation behavior result was compared with analytical deflection result based on composite laminate plate theory prior to overall structural analysis of the actuator embedded smart fins. Single bimorph piezoelectric actuator was analyzed with the clamped end under the operation condition of 400 V on x_3 direction using the present in-house analysis by MATLAB code based on composite

laminate plate theory. For its piezoelectric layer placed above the mid-plane of laminate, it applied bending deflecttion. Single bimorph piezoelectric actuator was analyzed with clamp end under the operation condition of 400 V in direction. For its piezoelectric layer placed symmetrically above and below the mid-plane of laminate, showed extensional deflection only when the same voltage was applied on both of the two piezoelectric layers of laminate. The bending deflection was induced when the opposite voltage were applied on each of those. Results are shown in Figs. 4.1 and 4.2 and summarized in Table 4.1.

Figure 4.3 shows the experimental deflection results of various bimorph actuators made of two different piezoelectric materials. 3203HD was previously used material for actuators and was used to compare with the PMN-29PT which was newly applied material for the actuator. PMN-29PT shows higher piezoelectric coefficient d_{31} which is related to the deflection along the principal axis. The maximum curvature deflection is 6.3° for the bimorph actuator under 400 V input. Result showed fairly linear relationship between voltage input and bending/extensional deflection, though slight discrepancy was observed. Such discrepancy resulted from the computation round off during the post-processing.

Significant difference between the bending and extensional deflection were observed. Experimental result of the bimorph actuator with single crystal piezoelectric material PMN-29PT regarding the actuation behavior showed 4.7 mm maximum bending deflection for 85 mm length bimorph, which is the rotation of 3.16° . The present in-house MATLAB simulation attempted to analyze the situation when applying voltage on both sides of the material, which was the same as twice the voltage input on each side. Experimental result showed good correlation with in-house simulation result shown in Table 4.1, which was twice result of the analytical prediction.

Although the ANSYS analysis had shown reasonable result compared to the analytical and experimental result, it is still unclear that it fully realized the piezoelectric characteristic of hysteresis. It is the energy loss via heat when piezoelectric material is actuated under voltage input and would result in decrease of maximum deflection on consecutive actuation under the same voltage input condition. Therefore, further study and analysis is required regarding hysteresis.

4. 2. Structural analysis of the present smart fins

Structural analysis for the whole fin structures containing the piezoelectric actuators was conducted using commercial finite element analysis software, ANSYS. ANSYS software supports static, transient, harmonic, and modal including pre-stressed modal analysis using linear perturbation. For static analysis, piezoelectric material properties such as structural elasticity, piezoelectric coupling, and dielectric permittivity are required to solve.

For the Design Candidate 2 and 3, hinge which is located on the 1/4 of the chord was fully restrained except for the axial rotation degree of freedom. All the actuators were given the voltage input condition of 400V on the upper component of single crystal piezoelectric actuator and 0 V on the lower component. In addition, computational fluid analysis were conducted for each design to derive the aerodynamic forces applied on the structure by using ANSYS Fluent software, thus ultimately resulting in structural behavior of the smart fins under aerodynamic loads.

4.2.1 Design Candidate 1

As the voltage input was given linearly from time 0 to 1 sec, the structure began to rotate on the pivot of 1/4 point of the chord length, showing linear deformation growth. (Fig. 4.4(a)) Angle of rotation of the fin was calculated by arctangent of (deformation of the tip/three quarter of the chord) and resulted in 2.31° .

Although the purpose of the design was to directly utilize the bending deflection of both unimorph and bimorph piezo-electric actuator, the result showed small deflection of 2.3° which cannot be considered applicable for the flight vehicle. In addition, as it can be seen on Fig. 4.4(b), upper skin had been detached from the original airfoil shape on maximum deflection state, which needs modification to keep it attached while actuating. Considering above characteristics of the design led to other design development.

4.2.2 Design Candidate 2

As the voltage input was given linearly from time 0 to 1 sec, the structure began to rotate on the pivot of 1/4 point of the chord length, showing linear deformation growth.(Fig. 4.5) Angle of rotation of the fin was calculated by arctangent of

(deformation of the tip/three quarter of the chord) and resulted in 5.83° .

For its simple structural components and mechanism, configuration and modification of the design was easier than Design Candidate 1 and showed higher deflection. However, for the long, slanted actuator shape it is assumed to be unstable during actual operation. In addition, at its maximum deflection state when lowering the trailing edge, upper side of the actuator is open to the possibility that it would make contact to the inner side of the pocket of the fin, thus limiting the deflection. Although it showed improved deflection value compared with that of Design Candidate 1, some refinement was necessary, which led to development of Design Candidate 3.

4.2.3 Design Candidate 3

With the linear increase of voltage input of 400V over 1 sec, maximum deformation was reached up to 5.45 mm on its tip on the trailing edge. (Fig. 4.6) The rotation angle result was 6.94° . By adopting the characteristic of the design by Barret [21] and modifying the actuator shape, bending angle had increased and overcome the possibility of contact between the

actuator surface and inner surface of the pocket of the fin structure.

Since it had shown fair deflection angle, actual flight condition was simulated to analyze the aerodynamic load at the instant of the deflection state.

Under the flight condition of Mach number 0.5, ideal gas, and inviscid flow, cross-sectional figure of Design Candidate 1 at its maximum deflection state was analyzed using ANSYS -Fluent. Aerodynamic analysis on design candidate 1 was simply the flow over the NACA0012 with change of angle of attack of 6.94° . Pressure distribution contour is shown in Fig. 4.7.

Structural behavior result was driven by applying the moment out of aerodynamic forces from the Fluent analysis result as shown in Figure 4.7. Resulting structural behavior under aerodynamic load after iterations showed 2.45° rotation angle with pivot on 1/4 of the chord. Total deflection of the trailing edge tip is shown in Figure 4.8.

4.2.4 Design Candidate 4

By applying novel mechanism of arranging bimorph actuators in crossing manner, the structure had shown promising

deflection angle. Although structure being separated in to three bodies connected by bimorph actuators and has contact sliding region by protruded skin might cause instability, it was worth analyzing for its fair performance itself.

With the linear increase of voltage input of 400V over 1 second on each of the embedded bimorph piezoelectric actuators, maximum deflection was reached to 20.7 mm on its tip on trailing edge. (Figure 4.9) Deflection angle was calculated by regarding the angle between chord line and the line connecting leading edge tip and trailing edge tip. The result was 12.97° .

Cross-section of the fully deflected airfoil was obtained from the side view of the deformed airfoil (Fig. 4.10(a)). Undeformed airfoil skins were adjusted to be attached to the body to make smooth curve as in Fig. 4.10(b) in order to derive the aerodynamic characteristics at its possibly maximum deflection shape by excluding the structural irregularities for later refinement. Pressure distribution contour is shown in Fig. 4.11.

Additional merit found was the ratio of the mass of piezoelectric material PMN-29PT used per structure is lowest among all four design candidates, which shows evident advantage regarding resource consumption. (Fig. 4.12)

Since Design Candidate 2 had shown promising result by showing high bending deflection, comprehensive structural behavior of the structure regarding flutter characteristics of the present fins based on the obtained modal analysis result as well as refining the protruded skins by applying mechanism that will smoothen the skin.

Since there also exist special sliding-contact regions in the present smart fin structures, it will be important to con-duct the contact analysis for frictional force estimation for more accurate analysis. Contact formulation will be investigated using analytical approach based on the plate element contact analysis suggested by Khostavi [27].

4. 3. Flutter analysis of the present smart fins

Since the present designs were to be applied on the flight vehicles, further examination over aerodynamic behavior such as flutter characteristics was planned. In order to find the flutter characteristics of a structure, their mode shape would be required. Thus those characteristics were analyzed in this thesis. Modal analysis of Design Candidate 3 and 4 was conducted using commercial structural analysis software MSC. NASTRAN and the results are shown in Figs. 4.13 and

4.15.

Further analysis condition was also derived for realistic approach. It is to consider the stiffness change of the piezoelectric material when actuated by voltage input. So far, the structure was considered as open circuit which has zero electric displacement over the electrode plating of the system during the actual operation. Closed circuit which has zero electric field on the system was also assumed to com-pare the flutter characteristics with that of the open circuit.

As expected by the theoretical approach using Eq. (2.2), Young's modulus of the closed circuit(12.8 GPa) was lower than that of the open circuit(18.5 GPa). By applying the altered material property for the modal analysis, result of the mode shapes were very similar to the open circuit mode shape. (Fig. 4.14)

By applying the properties above, flutter analysis of Design Candidate 3 was conducted using commercial analysis software, ZAERO.

Flight speed versus damping and frequency graphs for open circuit condition are shown in Figs. 4.16 and 4.17, respectively. It was seen that mode shapes were similar in both cases, however, with higher natural frequencies for open circuit condition.

Flutter analysis using ZAERO showed increase of the damping and became greater than zero at the point when the structure becomes unstable. As shown in Figs 4.16 and 4.17, flutter occurred on the 5^{th} mode (-■-) first when its damping increased and became greater than zero starting from velocity of 400 m/s, followed by 4^{th} (-△-), 8^{th} mode (-▲-), and 3^{rd} mode(-◇-) of open circuit condition (Fig. 4. 16). For the closed circuit condition, different characteristic was observed in Figs 4.17 where 4^{th} mode (-△-) showed instability boundary velocity of around 300 m/s. For the record, some modes such as mode 9 and 10 had shown local characteristics of bimorph actuator in the ZAERO analysis.

The result showed that flutter occurred at about 400 m/s and 300 m/s for open and closed circuit condition, respectively. Since the flight condition of the system was Mach number 0.5, subsonic environment, flutter occurrence of the structure in the flight speed above 300 m/s ensured stable behavior in given flight condition. Since Tube launched, Optically tracked, Wire-guided, TOW, missile was assumed for the application of the smart fin, air-to-surface (guided) missile condition was also concerned in addition to the ground-to ground missile condition as derived above. From the hover ceiling of 8000 ft [33] and

temperature of -0.83 ℃, air density 0.96 kg/m^3 was derived as initial flight condition. ZAERO input was adjusted accordingly and the result had shown very similar flutter behavior with about 50 m/s increase of flutter boundary for both open circuit (450 m/s) and closed circuit (350 m/s) condition, also showing
ensured stable behavior in given flight condition. (Figs. 4.18 and 4.19)

Comparison of the result for the fin structure under each circuit condition is shown in Table (4.2).

Future work will include the comparison of the modal analysis result of Design Candidate 3 with those obtained by the commercial software ANSYS, ZAERO, and Experimental result, thus validating the flutter analysis result, and flutter analysis of other design candidates.

Design Candidate 3 has aerodynamic advantage of constant aerodynamic pitching moment of the airfoil with respect to the angle of attack, which allows a variety of design attempts thus chosen to have potential of improvement of deflection angle magnitude. Flutter characteristics also show that the structure lies on stable region as far as it does not speed up beyond 440 m/s, which is higher value than the assumed normal operating flight condition of Mach number 0.5.

Although Design Candidate 4 was not fully analyzed to derive flutter characteristics, its highest deflection angle and used piezoelectric material per structure ratio indicates the design is worthy of further study.

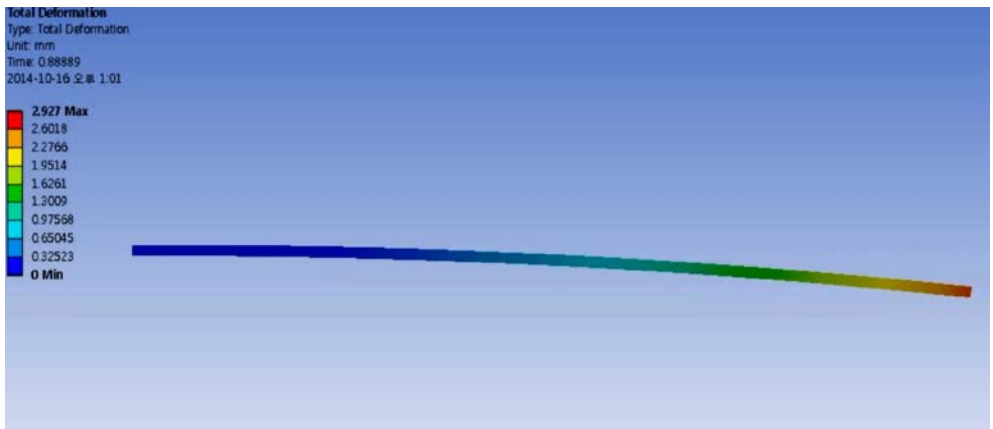

(a) Maximum deflection state of unimorph actuator

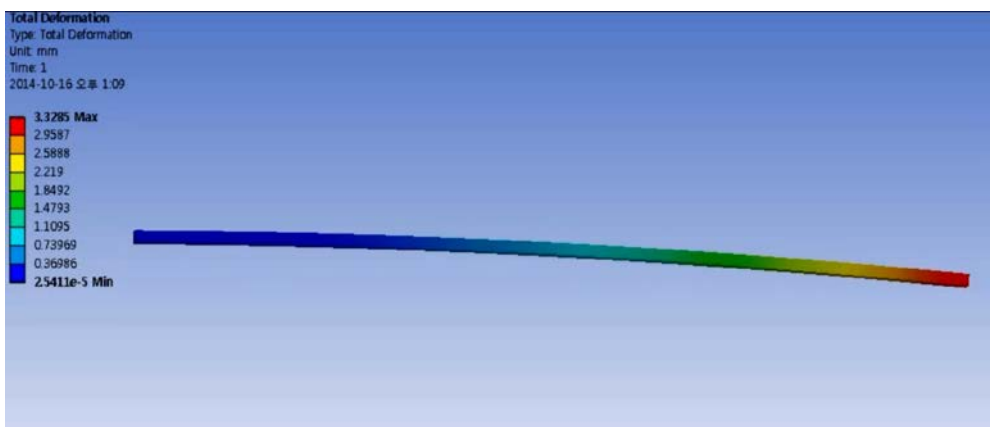

(b) Maximum deflection state of bimorph actuator

Figure 4.1 Deflection state of piezoelectric actuator used in Design Candidate 1

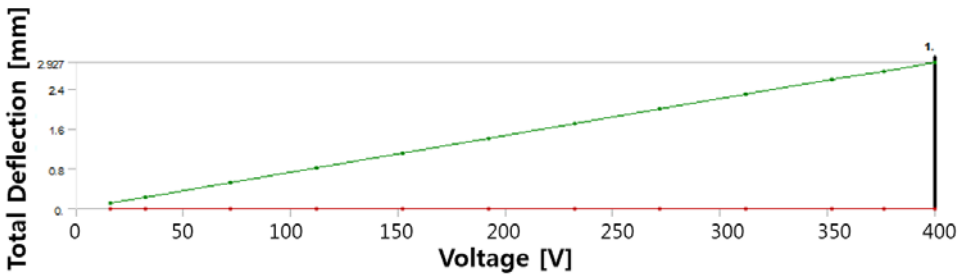

(a) Deflection with respect to voltage input of unimorph actuator

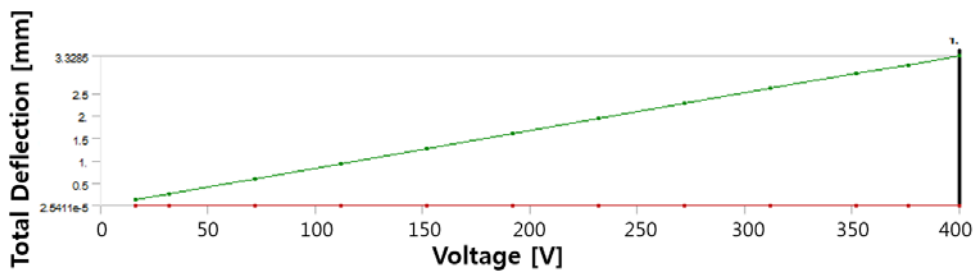

(b) Deflection with respect to voltage input of bimorph actuator

Figure 4.2 Deflection with respect to voltage input of actuators used in Design Candidate 1

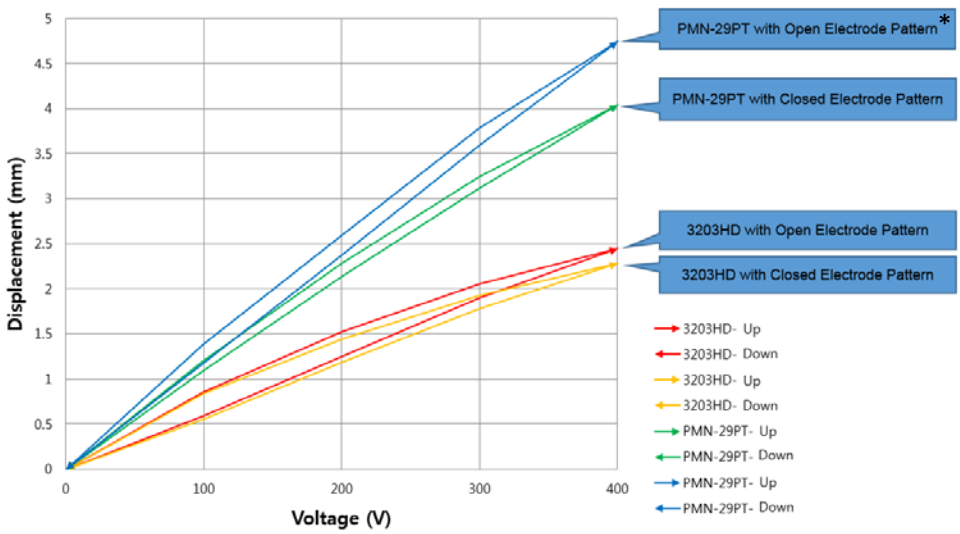

* PMN-29PT with Open Electrode Pattern was applied on the bimorph actuators of Design Candidate 1

Figure 4.3 Experimental deflection results of the various bimorph piezoelectric actuators

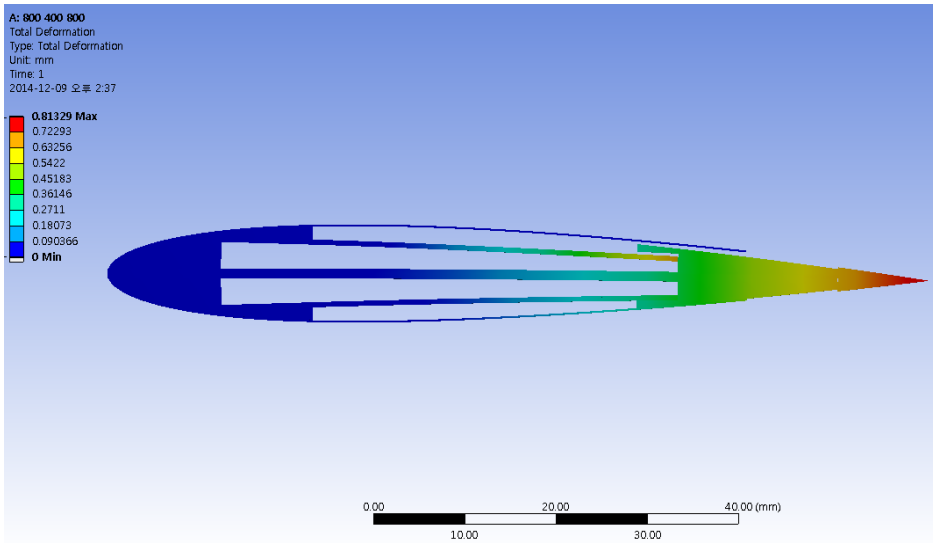

(a) Side view of Design Candidate 1 without external load

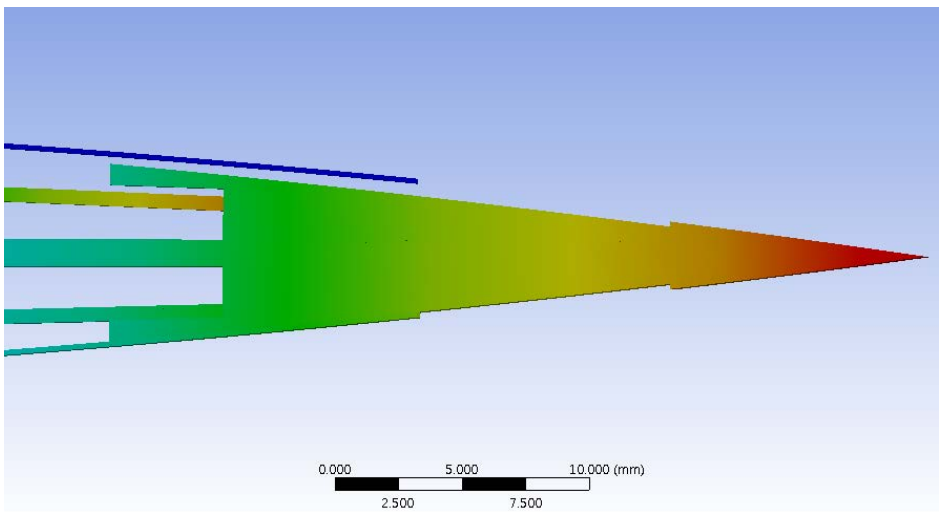

(b) Close-up on the trailing edge of the Design Candidate 1

Figure 4.4 Maximum deflection of Design Candidate 1 without aerodynamic load

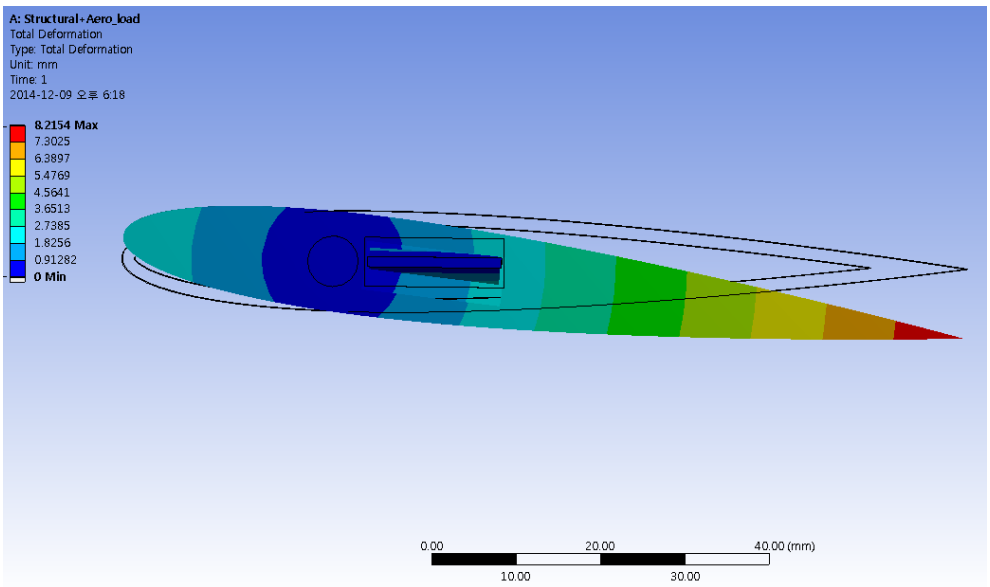

Figure 4.5 Maximum deflection of Design Candidate 2 without aerodynamic load

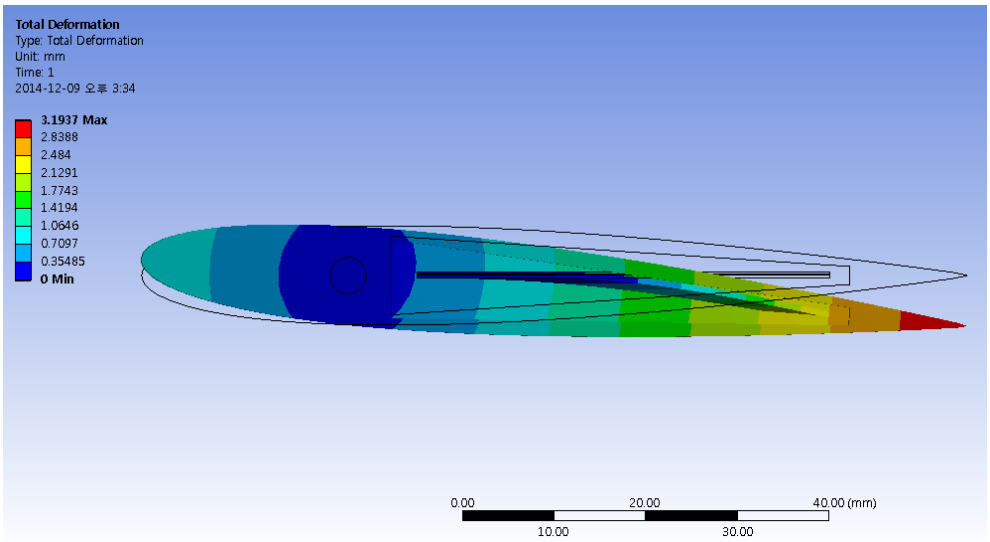

Figure 4.6 Maximum deflection of Design Candidate 3 under aerodynamic load

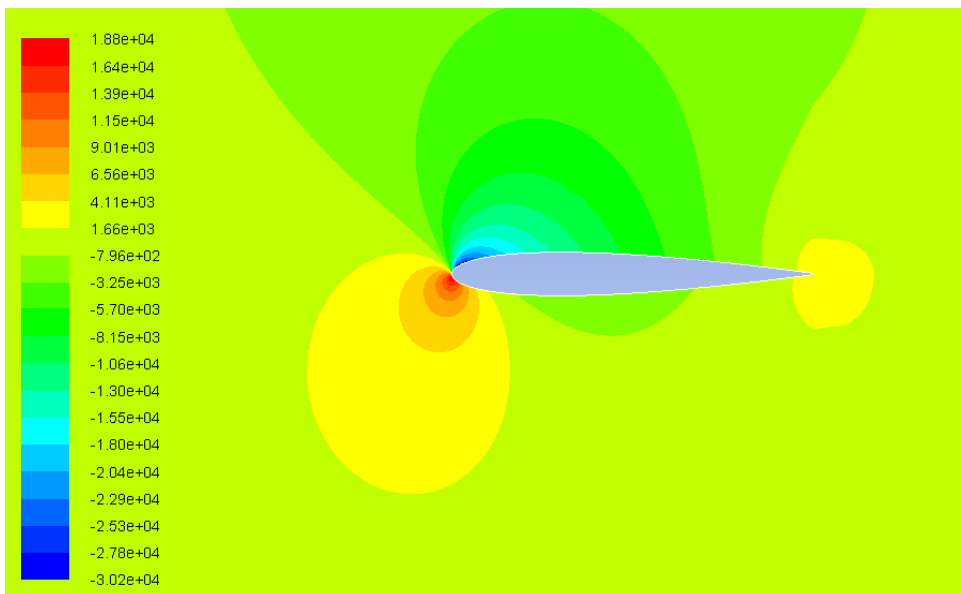

Figure 4.7 Pressure distribution of Design Candidate 3

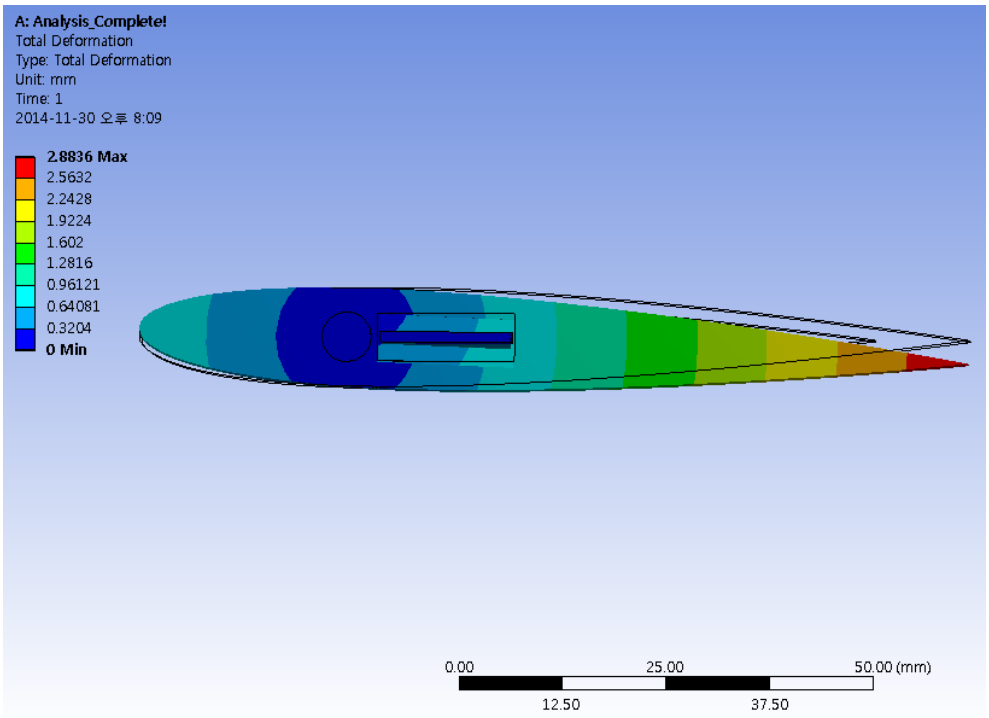

Figure 4.8 Maximum deflection of Design Candidate 3 under aerodynamic load

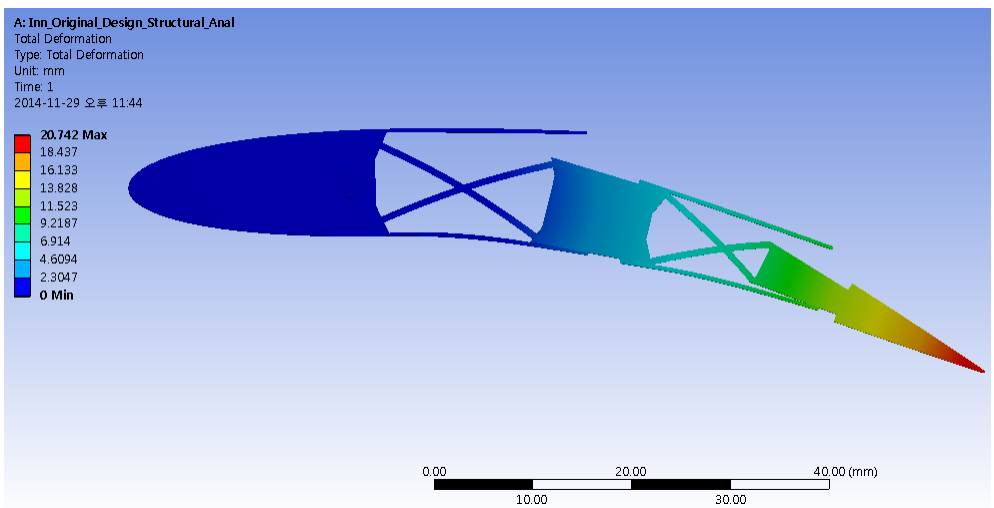

Figure 4.9 Maximum deflection shape of Design Candidate 4 without aerodynamic load

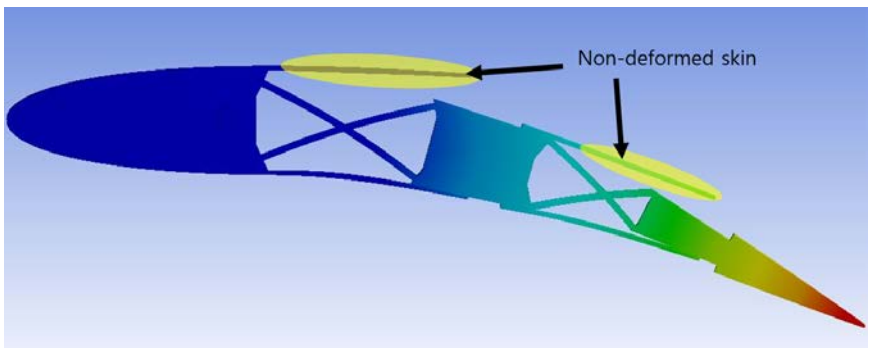

(a) Original deformed structure

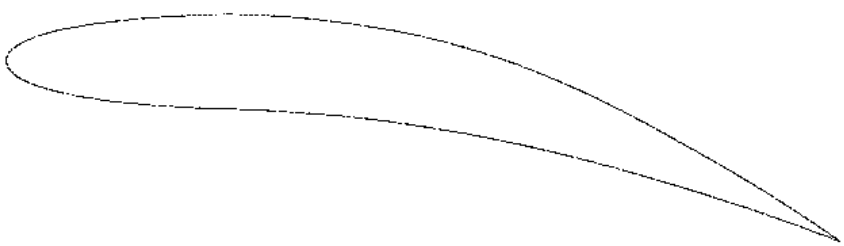

(b) Approximated cross-sectional contour

Figure 4.10 Cross-section and contour of Design Candidate 4 without aerodynamic load

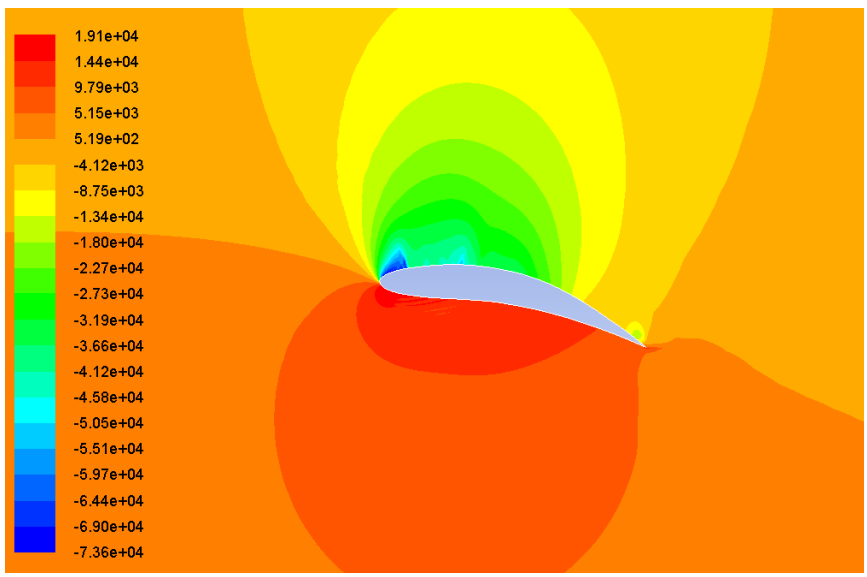

Figure 4.11 Pressure Distribution of the Design Candidate 4

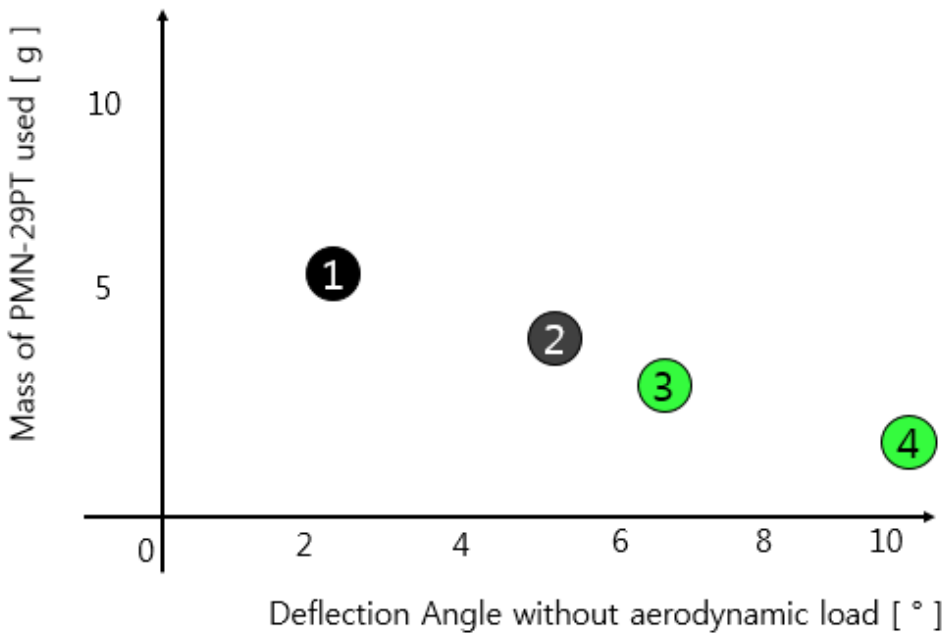

Figure 4.12 Mass of piezoelectric material used per structure ratio of all four design candidates

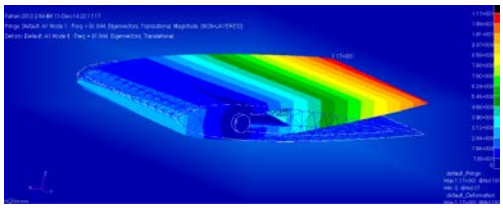

Mode 1 Freq. = 91.844 Hz

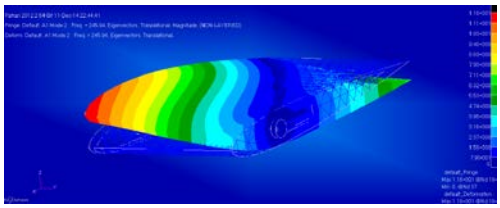

Mode 2 Freq. = 245.94 Hz

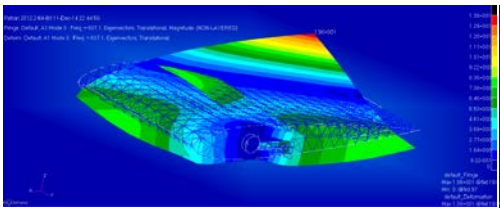

Mode 3 Freq. = 637.1 Hz

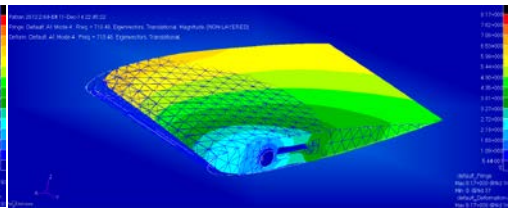

Mode 4 Freq. = 713.48 Hz

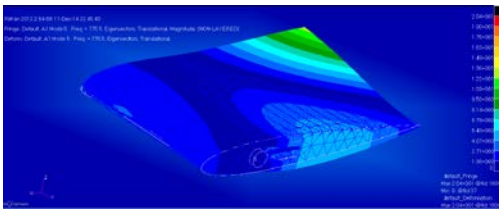

Mode 5 Freq. = 775.5 Hz

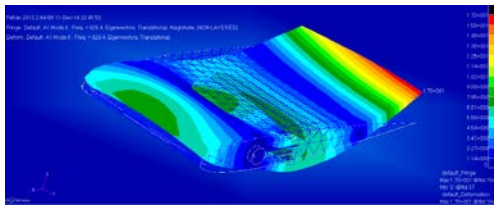

Mode 6 Freq. = 929.4 Hz

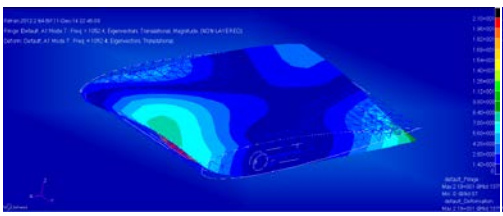

Mode 7 Freq. = 1052.4 Hz

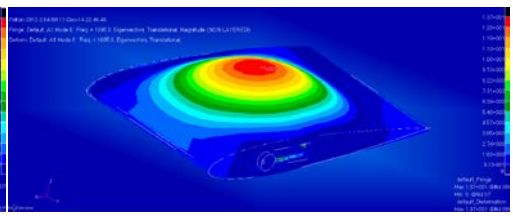

Mode 8 Freq. = 1095.3 Hz

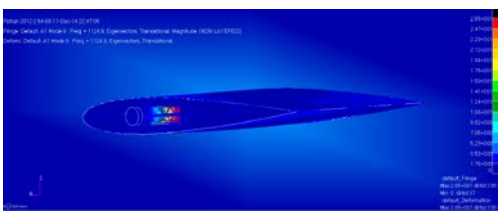

Mode 9 Freq. = 1124.9 Hz

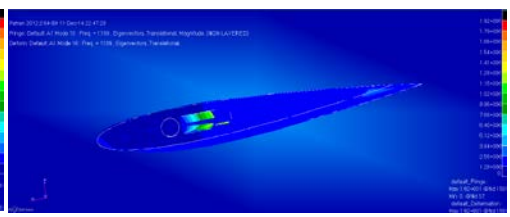

Mode 10 Freq. = 1189 Hz

Figure 4.13 Natural frequencies and mode shapes of Design Candidate 3 under open circuit condition

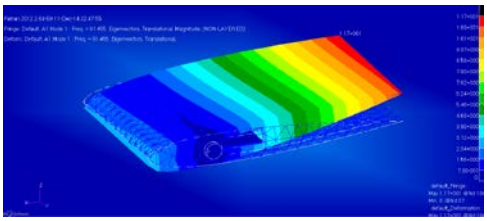

Mode 1 Freq. = 91.455 Hz

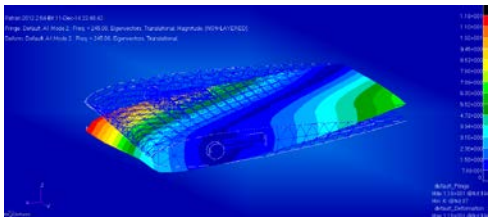

Mode 2 Freq. = 245.08 Hz

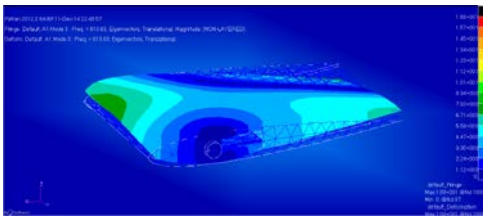

Mode 3 Freq. = 613.83 Hz

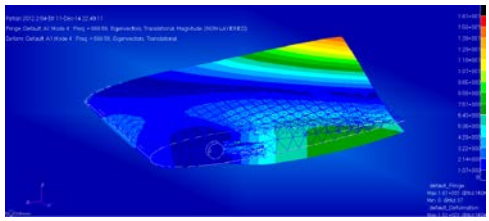

Mode 4 Freq. = 688.56 Hz

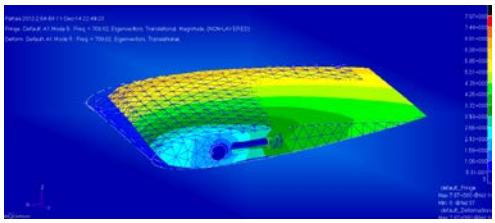

Mode 5 Freq. = 709.62 Hz

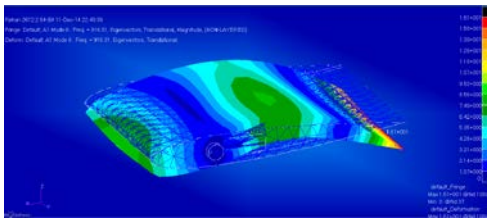

Mode 6 Freq. = 916.31 Hz

Mode 7 Freq. = 1013.3 Hz

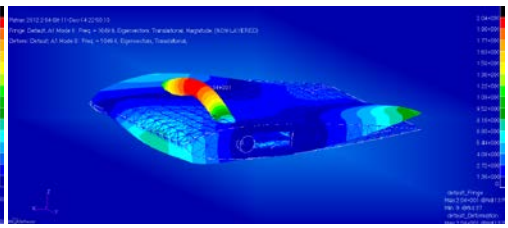

Mode 8 Freq. = 1049.6 Hz

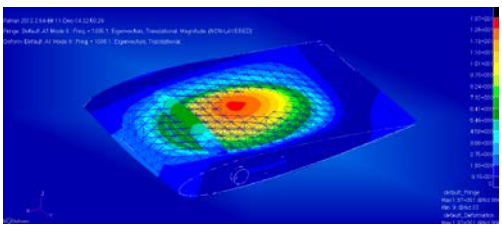

Mode 9 Freq. = 1095.1 Hz

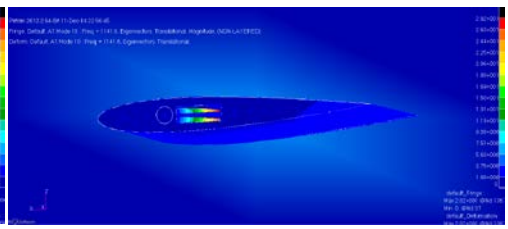

Mode 10 Freq. = 1141.6 Hz

Figure 4.14 Natural frequencies and mode shapes of Design Candidate 3 under closed circuit condition

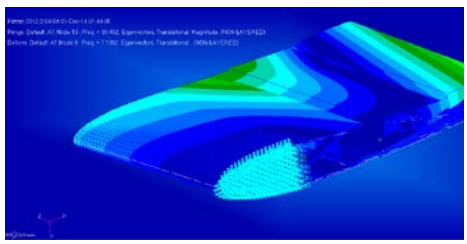

Mode 1 Freq. = 7.1362 Hz

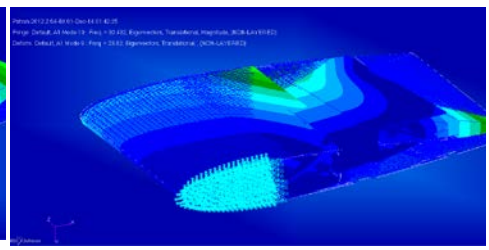

Mode 2 Freq. = 23.82 Hz

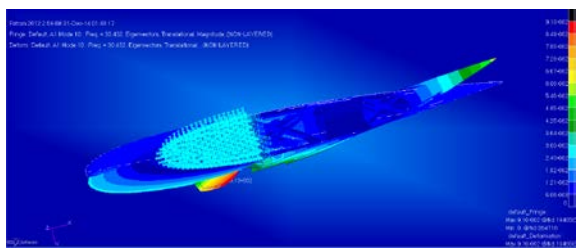

Mode 3 Freq. = 30.432 Hz

Figure 4.15 Natural frequencies and mode shapes of Design Candidate 4

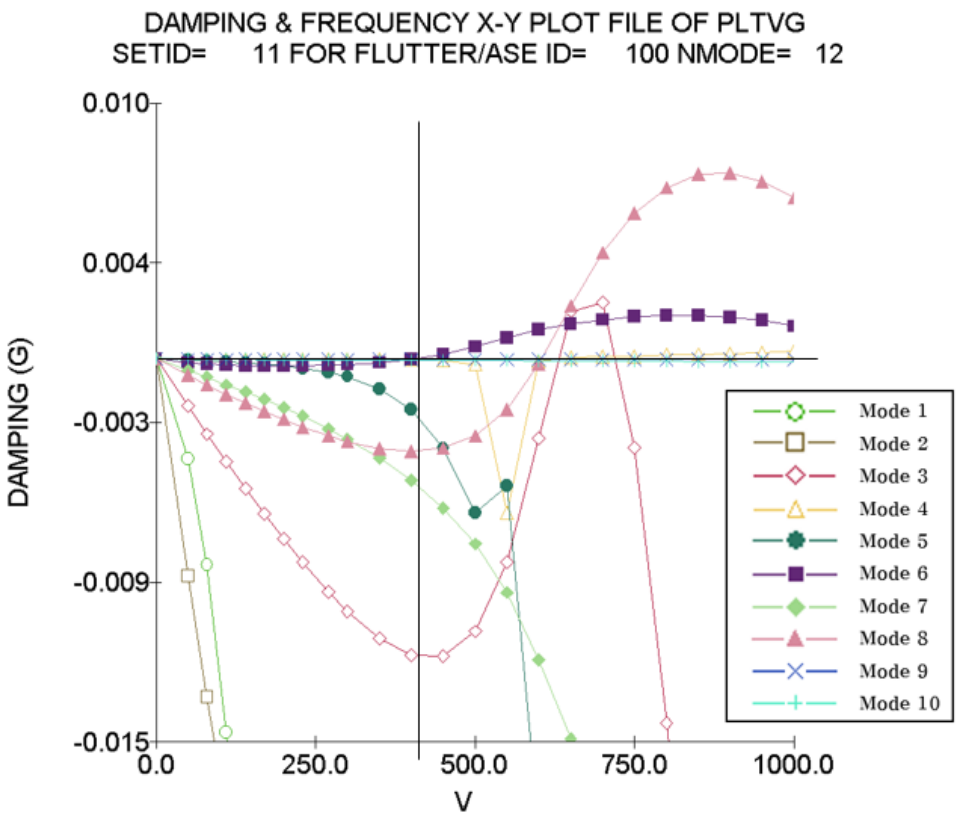

Figure 4.16 Flight Speed versus damping graph of Design Candidate 3 under open circuit condition as ground-to-surface condition

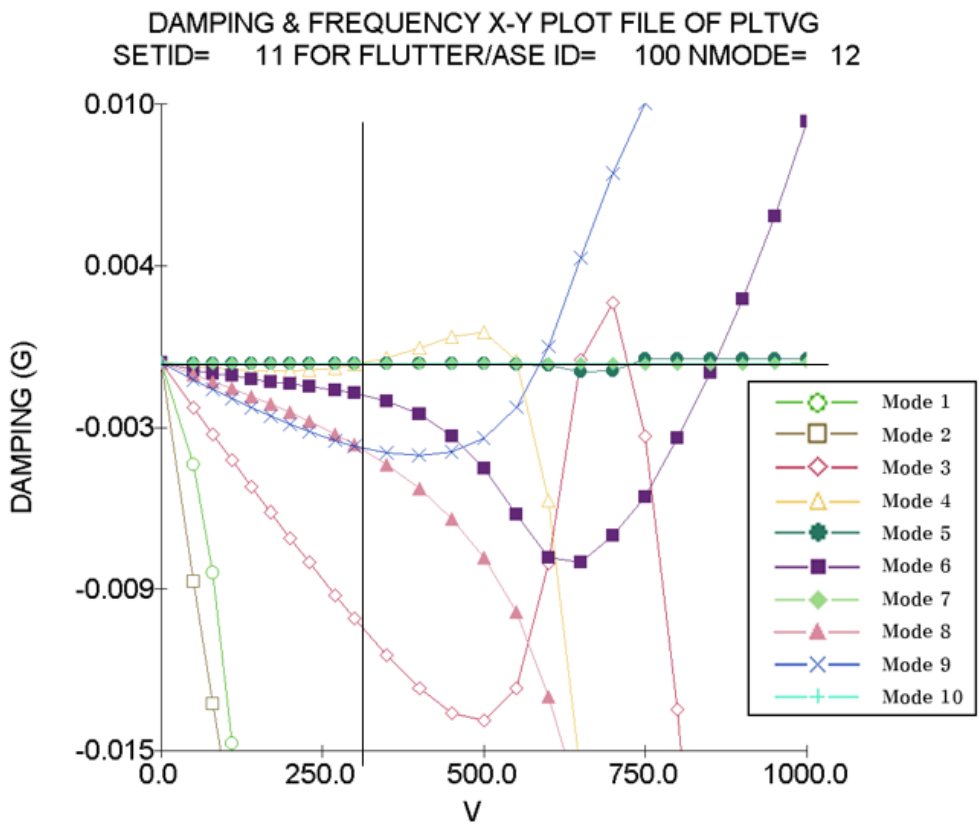

Figure 4.17 Flight speed versus damping graph of Design Candidate 3 under closed circuit condition as ground-to-surface condition

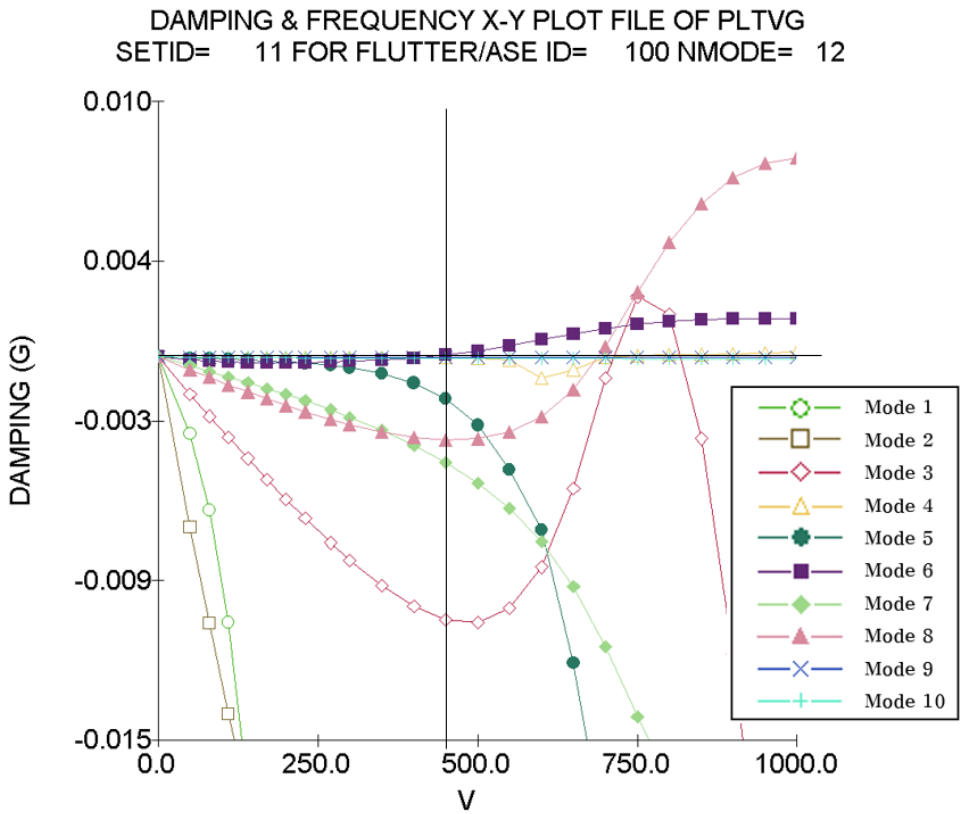

Figure 4.18 Flight speed versus damping graph of Design Candidate 3 under open circuit condition as air-to-surface condition

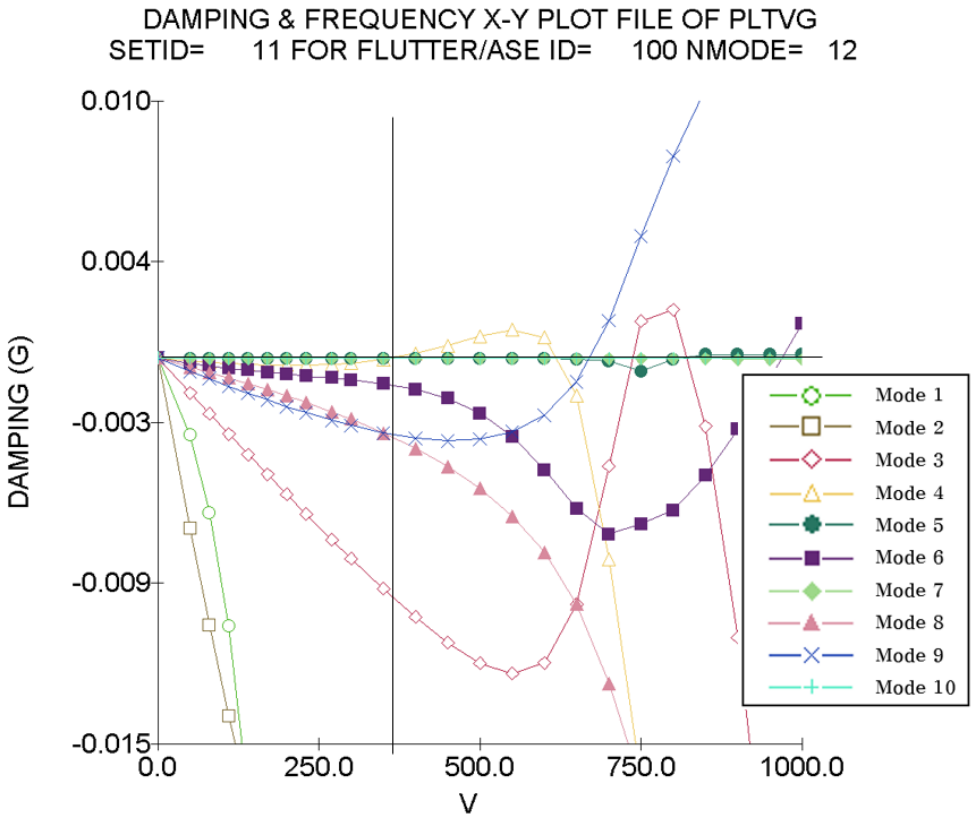

Figure 4.19 Flight speed versus damping graph of Design Candidate 3 under closed circuit condition as air-to-surface condition

Table 4.1 Analytical result using MATLAB for the bimorph piezoelectric actuators

a. 400 V

	Direction	Bimorph Opposite voltage[a] on each actuator
Extensional Displacement (mm)	1	0
	2	0
Curvature Displacement (°)	1	-6.3
	2	6.3

Table 4.2 Flutter analysis summary for two different circuit conditions

a. Modes which showed instability

b. Young's Modulus and Natuural Frequency does not change

		Young's Modulus (E_1) (GPa)	Natural Frequency[a] (mode 3, 4, 8, 9) (Hz)				Flutter Speed (m/s)
Ground to ground	Open Circuit	18.5	637.1	713.5	1052.4	1095.3	400
	Closed Circuit	12.8	613.8	688. 6	1049.6	1095.1	300
Air To ground[b]	Open Circuit	18.5	637.1	713.5	1052.4	1095.3	450
	Closed Circuit	12.8	613.8	688.6	1049.6	1095.1	350

Ⅴ. Conclusions

5.1 Conclusion

In this thesis, four composite smart fin structures with single-crystal piezoelectric material PMN-29PT embedded were analyzed in order to find their piezoelectric actuation-induced structural behavior under certain aerodynamic load condition using commercial analysis software MATLAB in-house code, ANSYS, MSC, NASTRAN, and ZAERO.

Actuation of the piezoelectric materials were analyzed under 400 V input on one of the two laminated piezoelectric materials using MATLAB in-house code and ANSYS structural analysis. Those predictions were compared with the classical laminate plate theory and the piezoelectric actuation stress vectors. And those were compared with the experimental result. Bending deflections induced by the piezoelectric actuation with respect to voltage input showed satisfactory linear relationship. Its experimental result for the maximum rotation for bimorph actuator also showed reasonable result compared to theoretical analysis.

Four smart fins were analyzed by realizing piezoelectric actuated structural behavior and then applied aerodynamic

load under Mach number 0.5, ideal gas, and inviscid flow condition with Design Candidate 3 and 4. Pressure distribution for each design at its maximum deflection state was also obtained to derive nodal forces regarding horizontal and vertical direction, which were applied on the smart fin designs.

Design Candidate 1 showed the deflection angle of 2.3° which was not enough for further analysis and application. Direct utilization of the bending deflection of both unimorph and bimorph piezoelectric actuator fell short of the expectation because of the actuators' inherent small deflection. In addition, skin of the structure had been detached, disrupting the original airfoil shape.

Angle of rotation of the Design Candidate 2 was resulted in 5.8° , which showed potential for application. Its simple structural aspects and mechanism showed merits compared to the other candidates. However, for the long, slanted actuator shape, contact between the inner surface of the fin structure was evident during actual operation, which would lead to limiting the deflection.

Design Candidate 3 was an improved design from Design Candidate 2 which was to rotate on the hinge of 1/4 of the chord length. The result showed slightly bigger rotation

angle of 6.9° without external aerodynamic load and 2.45° with it. The design was considered to have potential of deflection improvement by design refinement.

Flutter analysis of Design Candidate 3 using ZAERO showed unstable flight speed boundary above 300 m/s for the ground-to-ground TOW missile condition and 350 m/s for the air-to ground TOW missile condition. By this result, it is concluded that the fin under the assumed flight condition of Mach number 0.5 which is about 175 m/s did not experience the flutter and kept in stable condition for both operating conditions.

Design candidate 4 showed large deflection angle by amplifying small deflections induced by bimorph actuators embedded on two separate components. The rotation angle was predicted to be 12.9° without external aerodynamic load. Its overall deflection angle showed potential of further analytical, experimental study and refinement for stabilization and application. In addition, the mass of the PMN-29PT used in structure is least among all four design candidates.

Although Design Candidate 4 had shown the largest overall deflection of the smart fin with the best efficiency of amount of piezoelectric material per structure, flutter analysis is required to check its stability and solution for detaching skins

is yet to be clarified.

Design Candidate 3 had shown reasonable amount of deflection and stability under given aerodynamic condition by various simulation analysis, thus chosen among the four design candidates presented.

5.2 Future works

Based on the research presented in this thesis, following future works are recommended.

5.2.1 Design Refinement

Analysis and comparison of the deflection of the fin embedded with piezoelectric actuator of flight vehicle was the main purpose of this thesis. Four design candidates were presented by offering two distinguishing characteristics: rotating hinge, and morphing.

Further refinements will be made by applying optimally sized piezoelectric actuator with laminate lay-up which enables better performance with stability. Single crystal piezoelectric actuator is currently being experimented and expected to show improvement.

Each design can enhance its deflection performance by modifying the mechanisms interrelating the components of the structure. Design Candidate 3 showed promising result by showing resonable deflection angle. It showed possibility that mechanism design could affect the overall deflection angle. It was also shown that the structure's flutter boundary lies far from the given flight velocity, which verified its stability. However, there exists decreased of deflection angle by almost a half under aerodynamic load, which needs improvement. Improvement could be made by further optimization of the lay-up of bimorph actuator. Further work will include the design refinement regarding placement of the bimorph actuator as well as testing and verification of optimal size and lay-up of the piezoelectric actuator for Design Candidate 3.

5.2.2 Hysteresis Analysis

Since the structural analysis result of the given actuator had not fully realized piezoelectric actuation regarding hysteresis, it will be further studied and analyzed to be applied for better simulation of the structures. Previous research by Singh [34] regarding mathematical modelling and comparison with experimental result of piezoelectric actuator will

be taken into account for further hysteresis study.

5.2.3 Contact Analysis

In the present smart fin designs, there exist sliding-contact regions which confine the movement, thus controling the overall deflection. Therefore, it is important to analyze the contacting region with advanced approach. It was considered frictionless for the contacting regions of the designs presented in this thesis, thus only considering the actuation behavior of each smart fin. However, it will be necessary to consider the friction of the region for the realistic approach and result. This can be done by manipulating the options and variables in the commercial software, ANSYS. Advanced approach will also be made by using shell element, as previous research by Khostavi [27], based in-house code with theoretical approach of contact analysis such as augmented Lagrange method.

5.2.4 Flutter Analysis

In this thesis, flutter analysis for the Design Candidate 3 is presented. Similar research for the Designs presented will

require further refinements and structural analysis in advance. Since modal analysis is the basis of the flutter analysis, it is important to verify the simulated modal analysis result by commercial software, MSC. NASTRAN. Verification will be made by conducting modal analysis using other commercial software, ANSYS, and experiment. Further, for realistic approach, as also represented in this thesis for the Design Candidate 3 only, open circuit and closed circuit condition for the piezoelectric actuator will both be considered and compared for other designs such as Design Candidate 4 for it had shown fair result.

5.2.5 Comparison with experimental result

As presented in this thesis, piezoelectric actuator was simulated and its static structural characteristics were compared with the experimental result with fair correlation. Same verification will be made for the presented designs after their design refinements and amendment of realistic problems such as protruding skins when deflected of Design Candidate 4. Flutter analysis under aerodynamic flight condition simulated by wind tunnel will also be considered as well as operation testing of the structure without any loading.

References

1. Botelho, E. C., Silva, R. A., Pardini, L. C., and Rezende, M. C., "A Review on the Development and Properties of Continuous Fiber/Epoxy/Aluminum Hybrid Composites for Aircraft Structures", *Materials Research,* Vol. 8, No. 3, July/Sept. 2006.
2. Mangalgiri, P. D., "Composite Materials for Aerospace Applications", *Bulletin of Materials Science*, Vol. 22, Issue 3, pp. 657-664, May 1999.
3. Jaffe, B., Cook, W. R. Jr., and Jaffe, H., "Piezoelectric Ceramics", *Academic Press London and New York,* 1971.
4. Crawley, E. F., Luis J., "Use of Piezoelectric Actuators as Elements of Intelligent Structures", *AIAA Journal*, Vol. 25, No. 10, pp. 1373-1385, 1987.
5. Crawley, E. F., "Intelligent Structures for Aerospace: A Technology Overview and Assessment", *AIAA Journal*, Vol. 32, No. 8, pp. 1689-1699, 1994.
6. Baz, A., Poh, S., "Performance of an Active Control System with Piezoelectric Actuators", *Journal of Sound and Vibration*, Vol. 126, Issue 2, pp. 327-343, 22 Oct. 1988.
7. Uchino, K., "Piezoelectric Actuators and Ultrasonic Motors", *Kluwer Academic Publishers*, 1997.
8. Salamone, S., Bartoli, I., Rhymer, J., Scalea F. L., Kim, H., "Validation of the Piezoelectric Rosette Technique for

Locating Impacts in Complex Aerospace Panels", *Health Monitoring of Structural and Biological Systems*, Vol. 7984, San Diego, California, USA, March 6, 2011.

9. Sahin, M., Karadal, F. M., Yaman, Y., Kircali, O. F., Nalbantoglu, V., Ulker, F. D., Caliskan, T., " Smart Structures and Their Applications on Active Vibration Control – Studies in the Department of Aerospace Engineering, METU," *Journal of Electroceramics*, Vol. 20, Issue 3-4, pp. 167-174, 2008.
10. Rabinovitch, O. and Vinson, J. R., "Smart Fins: Analytical Modeling and Basic Design Concepts," *Mechanics of Advanced Materials and Structures*, Vol. 10, pp. 249–269, 2003.
11. Mehrabian, A. R., Y-K, A., "Optimal Positioning of Piezoeletric Actuators on a Smart Fin Using Bio-Inspired Algorithms", *Aerospace Science and Technology.* Vol. 11, Issues 2–3, pp. 174–182, March–April, 2007.
12. Seifert, A., Eliahu, S., Greenblatt, D., and Wygnanski, I., "Use of Piezoelectric Actuators for Airfoil Separation Control", *AIAA Journal*, Vol. 36, No. 8, pp. 1535-1537, 1998.
13. Rabinovigch, O., Vinson, J. R., "Smart Fins: Analytical Modeling and Basic Design Concepts", *Mechanics of Advanced Materials and Structures*, Vol. 10, pp. 249-269,

2003.

14. Rabinovitch, O., Vinson, J. R., “On the Design of Piezoelectric Smart Fins for Flight Vehicles”, *Smart Materials and Structures*, Vol. 12, pp. 686-695, 2003.
15. Mani, S., Singh, S. N., Parimi, S. K., Yim, W., Trabia, M., “Adaptive Rotation of a mart Projectile Fin Using a Piezoelectric Flexible Beam Actuator”, *Journal of Vibration and Control*, Vol. 11, No. 8, pp. 1085-1102, 2005.
16. Gern, F. H., Inman, D. J., and Kapania, R. K., “Computation of Actuation Power Requirements for Smart Wings with Morphing Airfoils,” 43rd AIAA/ASME/ASCE/ AHS/ASC Structures, *Structural Dynamics, and Materials Conference*, 22-25 April, 2002.
17. Chinnasamy, P., and Chen, Y., “Application of Computational Fluid Dynamics on Smart Wing Design,” 43rd AIAA Aerospace Sciences Meeting and Exhibit, Reno, Nevada, 10-13 Jan., 2005.
18. Bent, A. A., Hagood, N. W., Rodgers, J. P., “Anistropic Actuation with Piezoelectric Fiber Composites,” *Journal of Intelligent Material Systems and Structures*, Vol. 6, May, 1995.
19. Kim, D. H., Han, J. H., and Lee, I., "Application of Fiber Optic Sensor and Piezoelectric Actuator to Flutter Suppression", *Journal of Aircraft*, Vol. 41, No. 2, pp. 409-

411, 2004.

20. Raja, S., Pashikar, A. A., Kamesh J. V., “Flutter control of a composite plate with piezoelectric multilayered actuators”, *Aerospace Science and Technology*, Vol. 10, Issue 5, pp 435–441, July 2006.
21. Barrett, R., Gross, R. S., and Brozoski, F., "Missile flight control using active flexspar actuators," *Smart Materials and Structures,* Vol. 5, No.2, pp. 121-128, 1996.
22. Vlot, A, Gunnink, JW., “Fibre Metal Laminates”, *Kluwer Academic Publishers*, Dordrecht, The Netherlands, 2001
23. Gaudenzi, P., “Smart structures: Physical behavior, mathematical modelling and application”, *Wiley*, 2009
24. ANSYS INC., “Workbench – Mechanical Introduction 12.0”, Ch.4, May 5, 2009.
25. Anonymous, “ANSYS Fluent Theory Guide, Release 15.0”, ANSYS Inc, Nov. 2013.
26. Da Silva, Clarence W., “*Vibration: Fundamentals and Practice*”, CRC Press LCC, 1999.
27. Khostavi, P., Ganesan, R., and Sedaghati, R., “Corotational Non-linear Analysis of Thin Plates and Shells Using a New Shell Element,” *International Journal for Numerical Methods in Engineering,* Vol. 69, pp. 859-885, 2007.
28. Hornlund, M. and Papazoglu, A., “Analysis and measurements of vehicle door structural dynamic response”,

Divison of Structural Mechanics, Lund University, Sweden, 2005.

29. Anonymous, "Modal Frequency Response Analysis using MSC. NASTRAN", MSC Software Corporation.
30. Anonymous, "Theoretical Manual Version 9.0A", ZONA Technology INC., June, 2014.
31. Yoon, B. S., Yoon, K. J., "Design/Fabrication/Performance Test of UAV Actuator S-LIPCA with PMN-29PT Piezo-electric Single Crystal", *KSAS Conference*, pp. 985-988, Nov., 2013.
32. Lee, H. Y., "Material Constants of (011) PMN-29PT Single Crystals [Orthorhombic: mm2]", Ceracomp, March, 20, 2012
33. Anonymous, "MD 500E Flight Manual", MD Helicopters, Inc., 1998
34. Singh, A. K., Apte D., "Modelling and Analysis of Hysteresis in Piezoelectric Actuator", Defense Science Journal, Vol. 56, No. 5, pp. 825-833, Nov., 2006.

국문초록

본 논문에서는 유압으로 작동하는 기존의 조종익을 대체하기 위해 단결정 압전 구동 지능형 조종익 세 가지를 제시하였다. 설계된 조종익에 사용된 압전 구동기에 대한 구조 해석은 시뮬레이션 프로그램 ANSYS 의 해석 결과와 classical laminated plate theory 를 적용한 MATLAB in-house 코드를 활용한 이론적 결과, 그리고 실험 결과를 비교하였고, 이들 결과들은 일관성을 보였다. 특정 전압 조건에서의 조종익 설계들에 대한 구조 변형 특성을 예측하고 마하수 0.5 의 공력 조건에서의 부하를 고려한 구조 변형 특성 또한 예측하였다. 제시된 조종익의 설계와 해석들은 향후 유인 또는 무인 항공기의 날개 구조에 장착될 조종면부와 같은 실제 기술에 적용될 수 있을 것이다.

주요어 : 지능형 조종익, 압전 작동기, 구조 해석, 공력 해석

학 번 : 2013 – 20670